NAVAL POSTGRADUATE SCHOOL

MONTEREY, CALIFORNIA

THESIS

EFFECTS OF INTERNAL WAVES ON SOUND PROPAGATION IN THE SHALLOW WATERS OF THE CONTINENTAL SHELVES

by

Ming Yi Ong

September 2016

Thesis Advisor:	John E. Joseph
Second Reader:	Tetyana Margolina

Approved for public release. Distribution is unlimited.

THIS PAGE INTENTIONALLY LEFT BLANK

REPORT DOCUMENTATION PAGE			*Form Approved OMB No. 0704–0188*

1. AGENCY USE ONLY *(Leave blank)*	**2. REPORT DATE** September 2016	**3. REPORT TYPE AND DATES COVERED** Master's thesis

4. TITLE AND SUBTITLE
EFFECTS OF INTERNAL WAVES ON SOUND PROPAGATION IN THE SHALLOW WATERS OF THE CONTINENTAL SHELVES

5. FUNDING NUMBERS

6. AUTHOR(S) Ming Yi Ong

7. PERFORMING ORGANIZATION NAME(S) AND ADDRESS(ES)
Naval Postgraduate School
Monterey, CA 93943-5000

8. PERFORMING ORGANIZATION REPORT NUMBER

9. SPONSORING /MONITORING AGENCY NAME(S) AND ADDRESS(ES)
N/A

10. SPONSORING / MONITORING AGENCY REPORT NUMBER

11. SUPPLEMENTARY NOTES The views expressed in this thesis are those of the author and do not reflect the official policy or position of the Department of Defense or the U.S. Government. IRB number ____N/A____.

12a. DISTRIBUTION / AVAILABILITY STATEMENT
Approved for public release. Distribution is unlimited.

12b. DISTRIBUTION CODE

13. ABSTRACT (maximum 200 words)

Sound waves propagating through the oceans are refracted by internal waves. In the shallow waters of the continental shelves, an additional downward refraction of sound waves due to internal waves can cause them to interact more often with the seabed, resulting in additional energy from the sound waves being dissipated into the seabed.

This study investigates how internal waves affect sound propagation on the continental shelves. It first quantified the types of internal waves on the continental shelf of California, near Point Sal, using data collected from a field experiment. Next, the effects that these internal waves have on sound propagation were quantified via simulations using a ray theory acoustic model.

The results showed that internal waves in the experiment area were largely generated by tidal forcing. Compared to simulations without internal waves, simulations accounting for the effects of internal waves resulted in higher sound energy loss, as internal waves tend to cause sound waves to strike the seabed at steeper angles and over shorter distances. Thus, to enable a more accurate assessment of underwater acoustic system performance, the effects of internal waves on sound propagation in shallow waters need to be accounted for.

14. SUBJECT TERMS internal waves, shallow water, sound propagation, continental shelves	**15. NUMBER OF PAGES** 83
	16. PRICE CODE

17. SECURITY CLASSIFICATION OF REPORT	**18. SECURITY CLASSIFICATION OF THIS PAGE**	**19. SECURITY CLASSIFICATION OF ABSTRACT**	**20. LIMITATION OF ABSTRACT**
Unclassified	Unclassified	Unclassified	UU

NSN 7540–01-280-5500

Standard Form 298 (Rev. 2–89)
Prescribed by ANSI Std. 239–18

THIS PAGE INTENTIONALLY LEFT BLANK

Approved for public release. Distribution is unlimited.

EFFECTS OF INTERNAL WAVES ON SOUND PROPAGATION IN THE SHALLOW WATERS OF THE CONTINENTAL SHELVES

Ming Yi Ong
Military Expert 6, Republic of Singapore Navy
B.E.E., Nanyang Technological University, 2002

Submitted in partial fulfillment of the
requirements for the degree of

MASTER OF SCIENCE IN PHYSICAL OCEANOGRAPHY

from the

NAVAL POSTGRADUATE SCHOOL
September 2016

Approved by: John E. Joseph
Thesis Advisor

Tetyana Margolina
Second Reader

Peter C. Chu
Chair, Department of Oceanography

THIS PAGE INTENTIONALLY LEFT BLANK

ABSTRACT

Sound waves propagating through the oceans are refracted by internal waves. In the shallow waters of the continental shelves, an additional downward refraction of sound waves due to internal waves can cause them to interact more often with the seabed, resulting in additional energy from the sound waves being dissipated into the seabed.

This study investigates how internal waves affect sound propagation on the continental shelves. It first quantified the types of internal waves on the continental shelf of California, near Point Sal, using data collected from a field experiment. Next, the effects that these internal waves have on sound propagation were quantified via simulations using a ray theory acoustic model.

The results showed that internal waves in the experiment area were largely generated by tidal forcing. Compared to simulations without internal waves, simulations accounting for the effects of internal waves resulted in higher sound energy loss, as internal waves tend to cause sound waves to strike the seabed at steeper angles and over shorter distances. Thus, to enable a more accurate assessment of underwater acoustic system performance, the effects of internal waves on sound propagation in shallow waters need to be accounted for.

THIS PAGE INTENTIONALLY LEFT BLANK

TABLE OF CONTENTS

LIST OF FIGURES

THIS PAGE INTENTIONALLY LEFT BLANK

LIST OF TABLES

THIS PAGE INTENTIONALLY LEFT BLANK

LIST OF ACRONYMS AND ABBREVIATIONS

ADCP	Acoustic Doppler Current Profiler
cpd	Cycles Per Day
cph	Cycles Per Hour
CTD	Conductivity, Temperature, and Depth Sensor
IW	Internal Waves
ONR	Office of Naval Research
PDT	Pacific Daylight Time
psu	Parts Per Thousand
SD	Source Depth
SSP	Sound Speed Profile
Tx Loss	Transmission Loss
XBT	Expendable Bathythermograph

THIS PAGE INTENTIONALLY LEFT BLANK

ACKNOWLEDGMENTS

I would like to thank my thesis advisor, John Joseph, for giving me the leeway to scope the thesis toward a topic that would be relevant for my future work, for making possible a sea experiment to collect the relevant data, and for his advice and help in the data analysis and thesis writing process.

Thanks must also go to my second reader, Tetyana Margolina, for her help in the sea experiment and for providing insightful advice and edits toward making my thesis better and more "scientific."

Next, I would like to thank Thomas Rago, for his help in setting up the equipment for the sea experiment, and in ensuring that the experiment ran smoothly.

I would also like to give a big thanks to Professor John Colosi for his generosity in sharing the PSIEX experiment data and his analysis of the data, which were central for my work.

Lastly, I would like to thank my wife, Yi Tian, for taking care of the home front during our time here in Monterey, California, so that I could concentrate on my academic work.

THIS PAGE INTENTIONALLY LEFT BLANK

I. INTRODUCTION

Internal waves have been observed in many parts of the world's oceans (Jackson 2004, see Figure 1), and sound waves propagating through the ocean are refracted by these internal waves. In deep waters, such refraction generally only causes variability in transmission time (Marwoto 2015); it does not cause the sound waves to have additional sea-surface/seabed boundary interaction given the depth of the water column.

Figure 1. Locations of Observed Internal Waves. Source: Jackson (2004).

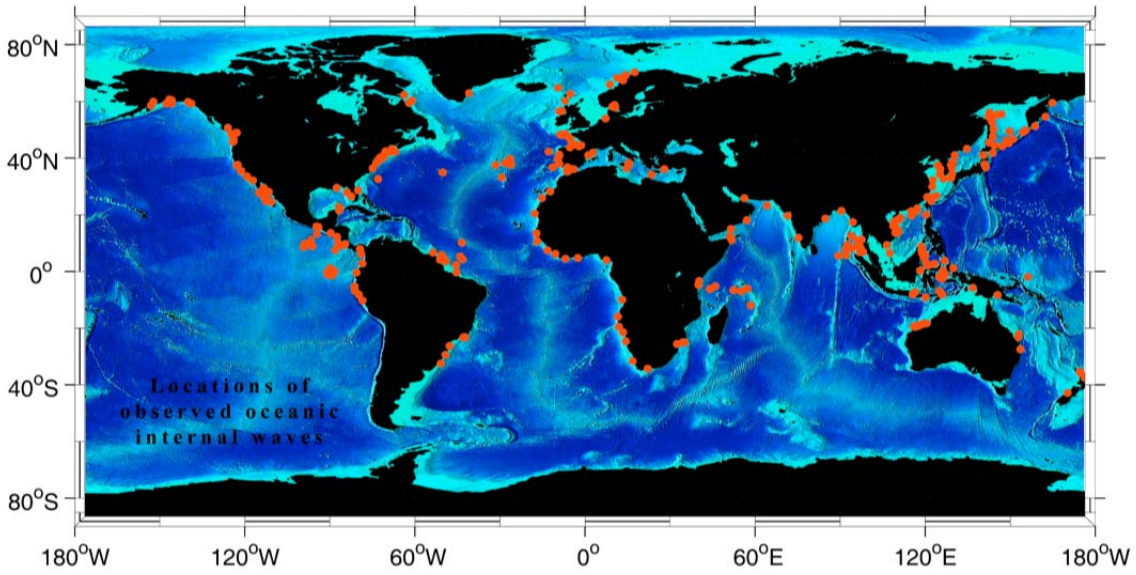

The red dots indicate the locations where internal waves are recorded in "An Atlas of Oceanic Internal Solitary Waves." The lack of observed internal waves in the open ocean is due to a lack of data at those locations.

In shallow waters such as the continental shelves however, an additional downward refracting of sound waves due to internal waves could cause them to interact more often with the seabed, causing greater transmission loss than would be expected in a scenario without internal waves, as additional energy from sound waves gets dissipated into or gets scattered by the seabed. Apel et al. (1997, 2007) have shown the importance of internal waves in shallow water acoustics, while Zhou et al. (1991) have shown 25 dB signal fluctuations in the Yellow Sea with timescales of minutes to hours.

The objectives of this thesis are to identify the types of internal waves in the shallow waters of a continental shelf and to analyze the effects they have on sound propagation ranges. The internal wave data were obtained from an Office of Naval Research (ONR)-sponsored experiment titled "2015 Point Sal Inner-shelf Experiment (PSIEX)," which was conducted in the coastal waters off Point Sal, California. The internal waves were measured using vertical strings of temperature sensors, while their effects on sound propagation ranges were quantified via simulations using a ray theory acoustic model called BELLHOP. The end goal is to do a generic study to determine how internal waves affect sound propagation ranges in the shallow waters of the continental shelves.

II. PHYSICAL BACKGROUND

A. WHAT ARE INTERNAL WAVES?

Internal waves (IW) are gravity waves that oscillate in water, rather than on the sea surface. An analogy would be a layer of oil sitting on a layer of water—a small shake of the mixture will create waves at the oil-water interface. In order for internal waves to exist there must be an increase in sea-water density with increasing depth, so that any perturbation would then cause an underwater wave to ripple outward as internal waves.

B. INTERNAL WAVES MANIFESTED AS WATER TEMPERATURE CHANGES

In the linear equation of state, density (ρ) is inversely proportional to temperature (T) and proportional to salinity (S).

Linear Equation of State: $\frac{\rho - \rho_0}{\rho_0} = -\alpha(T - T_0) + \beta(S - S_0)$,

where ρ_o =1025 kg/m^3, S_o = 35p su, T_o=10 °C, α = 2x10^{-4} °C^{-1}, β = 7.5x10^{-4}; α is the thermal expansion coefficient and β is the coefficient of saline contraction.

For this study, a constant salinity throughout the water column was assumed, as there was no introduction of fresh water into the region. Hence, temperature changes were the only factor contributing to changes in density in this investigation of internal waves. As deeper waters are usually colder than shallower waters, this implies that they are also denser than shallower waters. Thus, any external forcing would set up a wave at the interface between the waters of different temperature (and density). In other words, an internal wave, which propagates as perturbations in the density difference of water, is manifested and can be recorded as changes in water temperature.

C. TYPES OF INTERNAL WAVES IN THE SHALLOW WATERS OF THE CONTINENTAL SHELVES

1. Internal Tides—Internal Waves Generated by Tidal Forcing

Gerkema and Zimmerman (2008) show that internal waves on the continental shelves are generated by tidal forcing over the depth transition between the deep ocean and the shallow continental shelves. In this scenario, the internal waves have a semi-diurnal frequency of two cycles per day (cpd). This agrees well with our experiment observations where over a period of one day, two internal waves due to tidal forcing were observed (Figure 2). Internal waves generated by tidal forcing are also called internal tides.

Very often, a steep interface can occur between the cold and warm front of an internal wave. Such a steep interface is called a tidal bore or, simply, bore (see Figure 2).

Figure 2. Types of Internal Waves Observed in One Day.

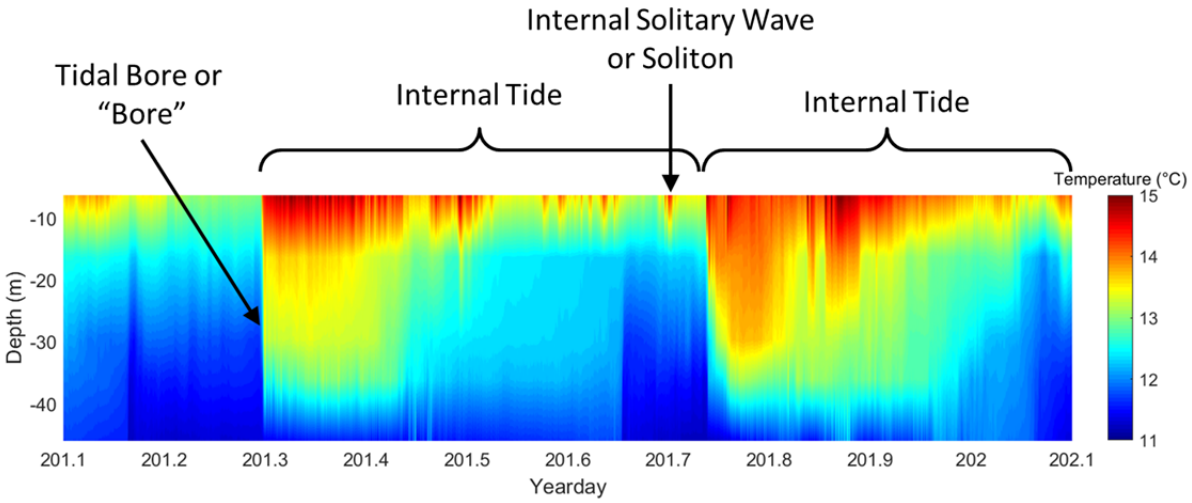

2. Solitons—Solitary Internal Waves

In addition to internal tides, shorter duration internal waves were observed throughout the data. These short spikes of internal waves are called internal solitary waves or solitons (Figure 2), which are generated from internal tides transferring their energies to shorter-space scales (Gerkema and Zimmerman 2008).

D. SEABEDS AND THEIR EFFECTS ON SOUND PROPAGATION

The types of seabed in shallow waters play a primary role in determining the range of sound propagation, as the waters in these areas are usually downward refracting and will cause sound to interact with the seabed multiple times over short distances (Jensen et al. 1994). Figure 3 illustrates this effect.

Figure 3. Ray Trace of a Horizontally Launched Ray in Mid-water Column.

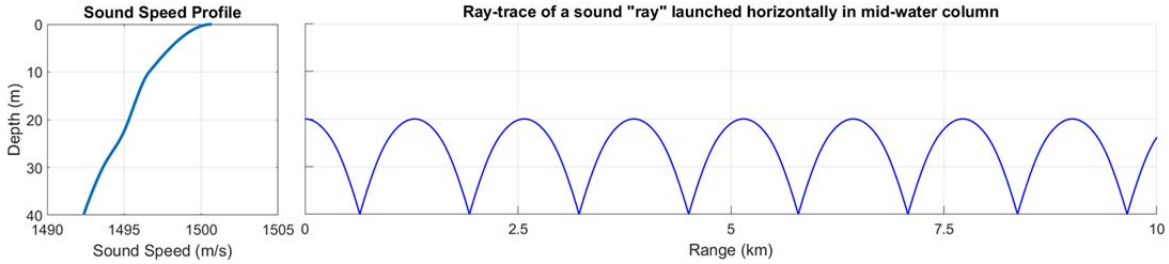

Left: A typical slightly downward refracting sound speed profile recorded during the experiment was used in the ray trace simulation run as shown to the right.

Right: A mid-water column horizontally launched sound "ray" gets refracted downward and interacts with the seabed eight times in 10 km.

Three representative continental shelf seabed types were used in the simulation runs: rocky seabed (chalk), sandy seabed (sandy-slit), and muddy seabed (clay-mud). The detailed parameters of each bottom characteristic used in the BELLHOP runs are listed in Table 1.

Table 1. Bottom Types Parameters Used in BELLHOP Runs. Adapted from Colosi (2016).

Bottom Type	Compressional sound speed (m/s)	Density (kg/m^3)	Attenuation (dB/λ)
Rocky (chalk)	2400	2200	0.2
Sandy (sandy-silt)	1644	1769	1.22
Muddy (clay-mud)	1470	1312	0.09

To understand the effects of bottom interaction on acoustics energy, it is necessary to invoke the formula for reflection coefficient to determine how much of the original ray intensity was reflected from the seabed at various grazing angles.

$$\text{Reflection coefficient: } R_{12} = \frac{m\sin\theta_g - \sqrt{n^2 - \cos^2\theta_g}}{m\sin\theta_g + \sqrt{n^2 - \cos^2\theta_g}} \ ,$$

where θ_g is the sound ray grazing angle as measured from the seabed plane, $m = \frac{\rho_2}{\rho_1}$, $n = \frac{c_1}{c_2}$, ρ_1 and ρ_2 are seawater and seabed density, respectively, and c_1 and c_2 are sound speed in seawater and seabed, respectively.

It should be noted that while all the seabed types are denser than seawater (approximately 1025 kg/m^3), the sound speeds in rocky and sandy seabed are faster than seawater (approximately 1500 m/s), while the sound speed of a muddy seabed is slower than that of seawater. This has important physical implications—for the rocky and sandy seabed, total internal reflection ($|R_{12}| = 1$) occurs when the direction of sound propagation (or a sound "ray") strikes the seabed at angles, $\theta_g \leq \theta cr$, where θcr (critical angle) is the highest angle at which total internal reflection can occur (Figure 4). As for the case of a muddy seabed, total internal reflection does not occur as there is no critical angle. Instead there is what is called a Brewster or intromission angle where $|R_{12}| = 0$, in which all energy from the sound waves in water gets dissipated into the seabed when θ_g is at the Brewster angle.

Figure 4. Reflection Coefficients of Rocky, Sandy, and Muddy Seabeds for the Various Grazing Angles.

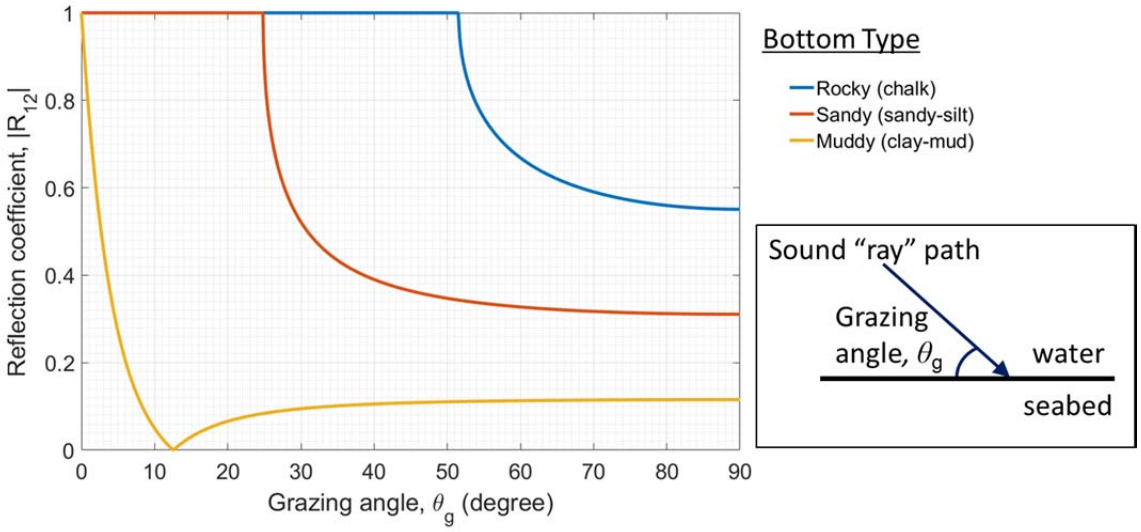

A sound "ray" is a vector that is normal to the sound wave front and which traces the path that a sound wave travels.

Referring to Figure 4, the rocky seabed has the highest critical angle of approximately 52°; hence, any sound ray striking a rocky seabed at less than that angle will experience total internal reflection. In fact, more than 55% of the sound energy will be reflected even when sound strikes the seabed at a 90° grazing angle. This means that the rocky seabed will allow sound to travel the farthest as it is the least lossy of the three seabeds.

For a sandy seabed, the critical angle is much smaller compared to the rocky seabed at approximately 25°. At grazing angles greater than the critical angle, the portion of reflected energy quickly drops to below 40% at grazing angles of above 40°. Hence, a sandy seabed is more lossy compared to a rocky seabed, and sound experiences more attenuation when it interacts with a sandy seabed.

For the muddy seabed, the percentage of energy reflected drops very rapidly from 100% at 0° grazing angle to 20% at 6° grazing angle. The Brewster angle is reached at approximately 12.5° grazing angle, and all the energy from the sound waves gets absorbed into the seabed. Beyond the Brewster angle, up to 90° grazing angle, only approximately 12% of the sound energy gets reflected back into the water. Hence, a

muddy bottom is extremely lossy, and sound will experience the most attenuation in this environment.

The simulated transmission loss plots for the three seabed types are as shown in Figure 5. The plots were generated using the sound speed profile (SSP) of Figure 3, and the only difference between the three plots is the seabed type. From the transmission loss plots, it is apparent that a rocky bottom has the least sound energy transmission loss, while a sandy bottom has more transmission loss and a muddy bottom has the most transmission loss.

Figure 5. Transmission Loss Plots for a Rocky Seabed (top), a Sandy Seabed (center), and a Muddy Seabed (bottom).

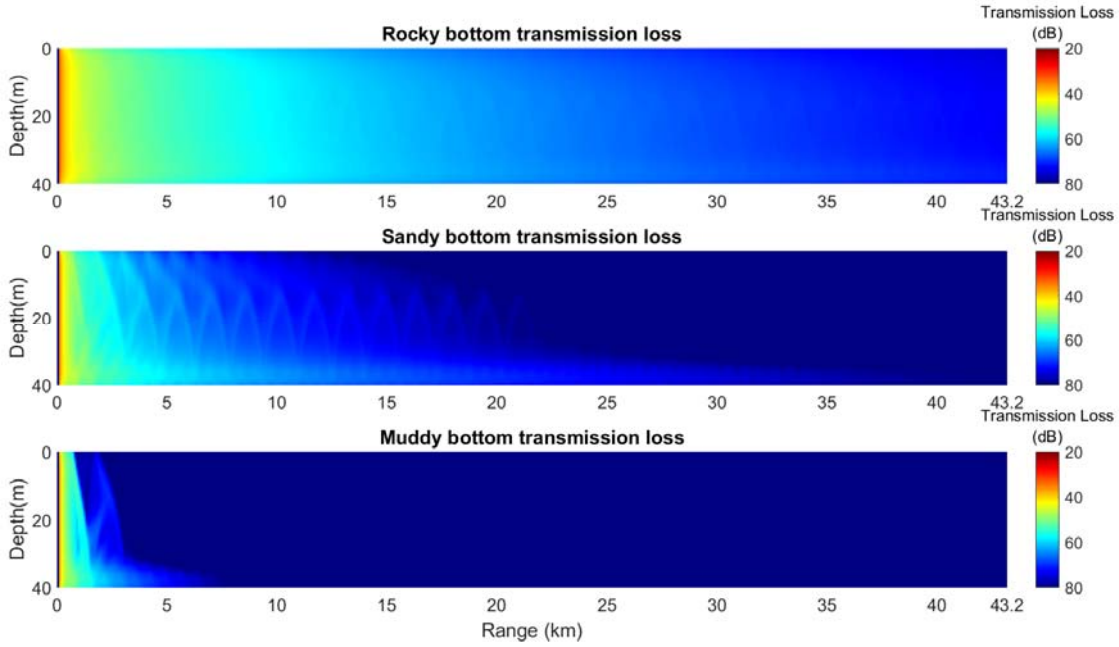

III. EXPERIMENT OVERVIEW

The data used in this investigation was collected during an ONR-sponsored effort titled "2015 Point Sal Inner-shelf Experiment (PSIEX)." The objective of the experiment was to quantify the various oceanographic phenomena in the coastal inner-shelf. The experiment took place in the waters off Point Sal, California, during the summer of 2015.

The locations of the various sensors are as shown in Figure 6. The experiment lasted 52 days from 15-Jun-2015 07:00 PDT (yearday 166.29) to 06-Aug-2015 07:00 PDT (yearday 218.29).

Figure 6. Experiment Site Sensor Deployment Locations.
Source: Colosi et al. (2016).

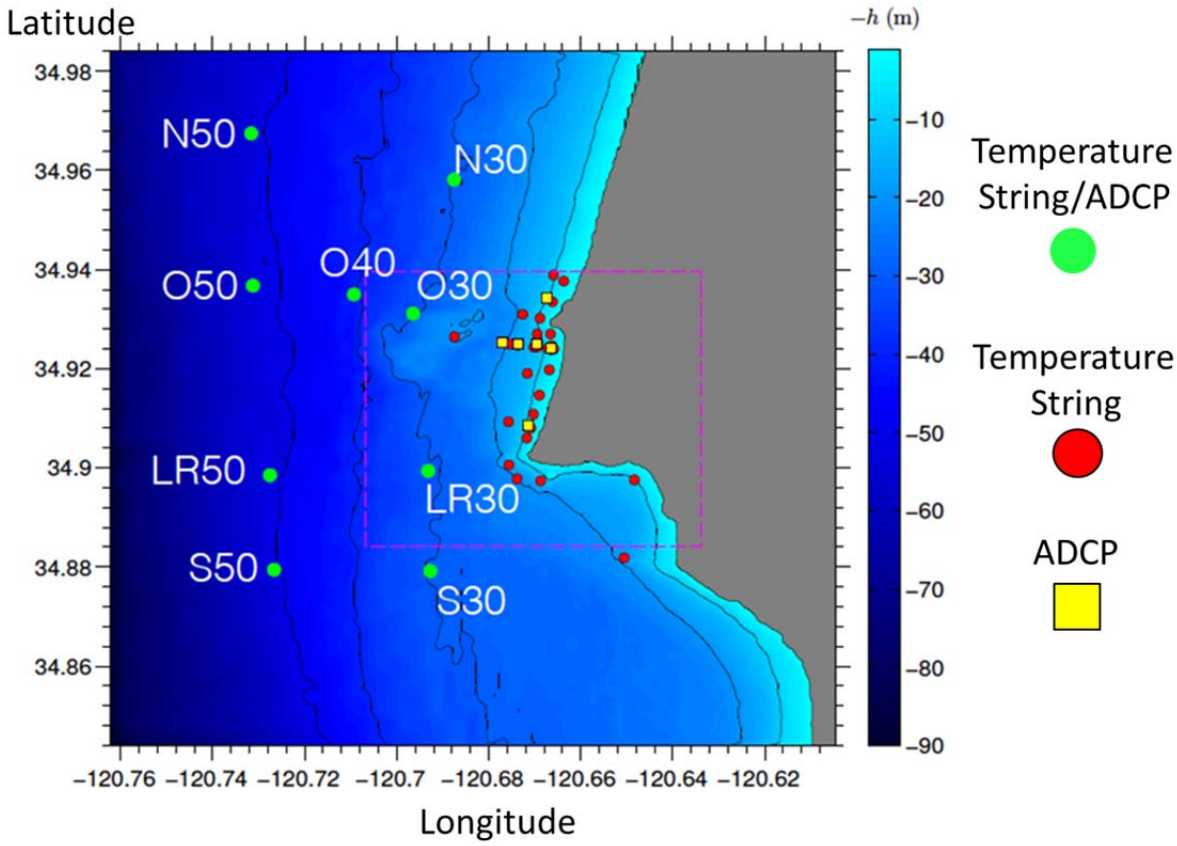

For this study, the focus was on temperature string O50, as it was the deepest deployed sensor of the experiment at 52 m water depth. Temperature string O50 consisted of five temperature sensors deployed from a depth of 6.2 m to 46.1 m at approximately 10 m spacing, and the water temperature was sampled once every 30 seconds (or 120 samples per hour). This allowed an internal wave frequency of up to 60 cph to be sampled, based on Nyquist–Shannon sampling theorem, which states that for a waveform to be accurately sampled, the sampling frequency must be two times that of the sampled waveform's highest frequency.

The maximum vertical oscillating frequency of internal waves is limited by the Brunt-Väisälä frequency, or buoyancy frequency, and any external forcing of a water column at a frequency that is higher than the Brunt-Väisälä frequency will not generate internal waves. Robert and William (1983) observe that the typical Brunt-Väisälä frequency in shallow water is 12–15 cph. Thus, the temperature sensor sampling rate of 120 samples per hour is adequate for observing the internal waves expected in this environment.

IV. CHARACTERISTICS OF INTERNAL WAVES IN THE EXPERIMENT AREA

A. OVERVIEW OF THE ENTIRE TEMPERATURE TIME SERIES

The recordings of temperature string O50 as a function of depth and time are shown in Figures 7a–h, with Figures 7a–g each showing one week of data and Figure 7h showing three days of data from week 8.

Figure 7. Temperature Plots of Temperature String O50 for the Entire Experiment (Figures 7a–h).

Figure 7a. Temperature Plot—Week 1.

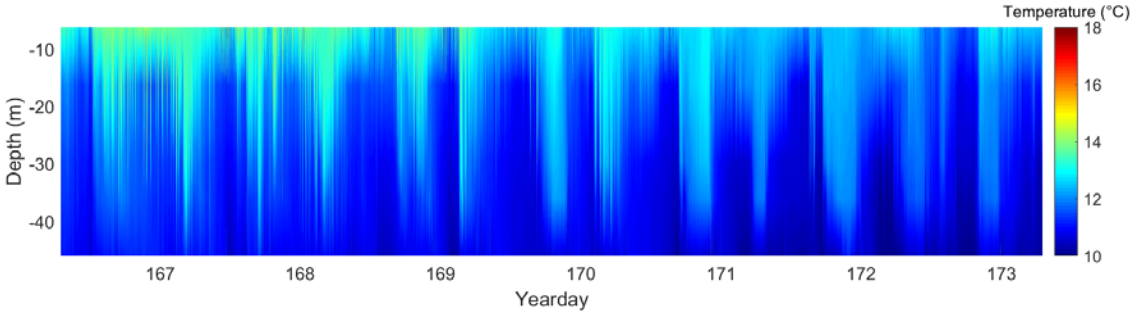

Figure 7b. Temperature Plot—Week 2.

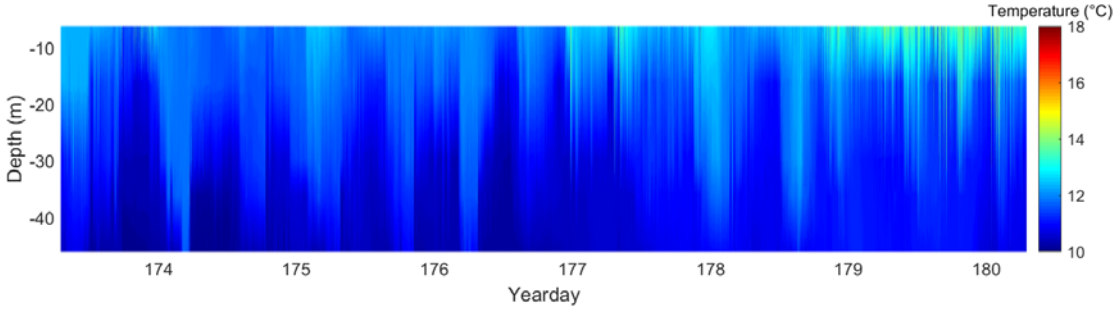

Figure 7c. Temperature Plot—Week 3.

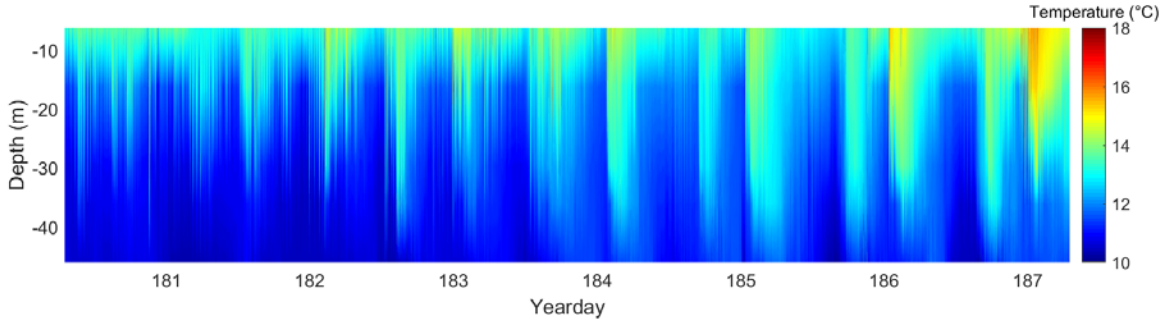

Figure 7d. Temperature Plot—Week 4.

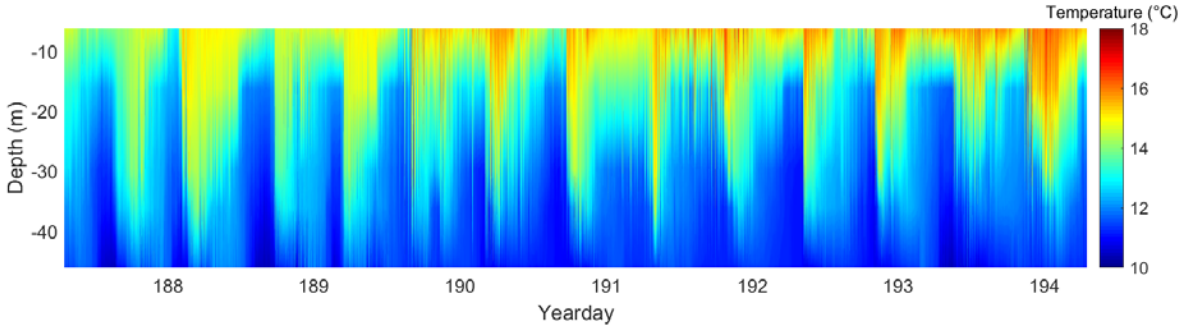

Figure 7e. Temperature Plot—Week 5.

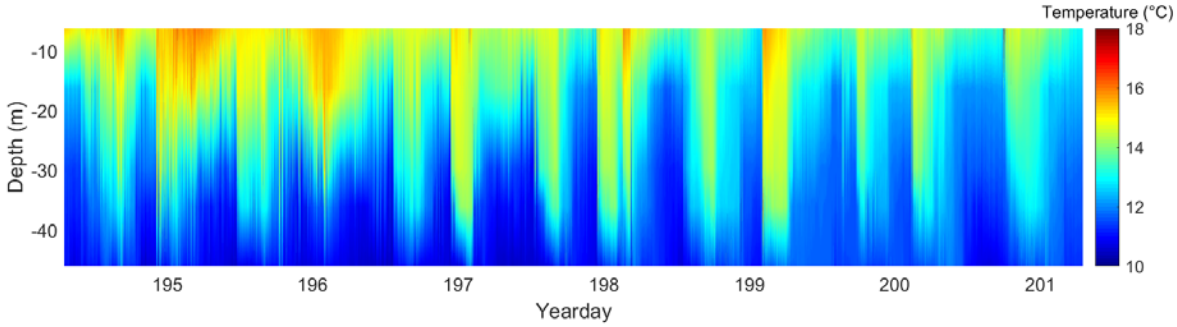

Figure 7f. Temperature Plot—Week 6.

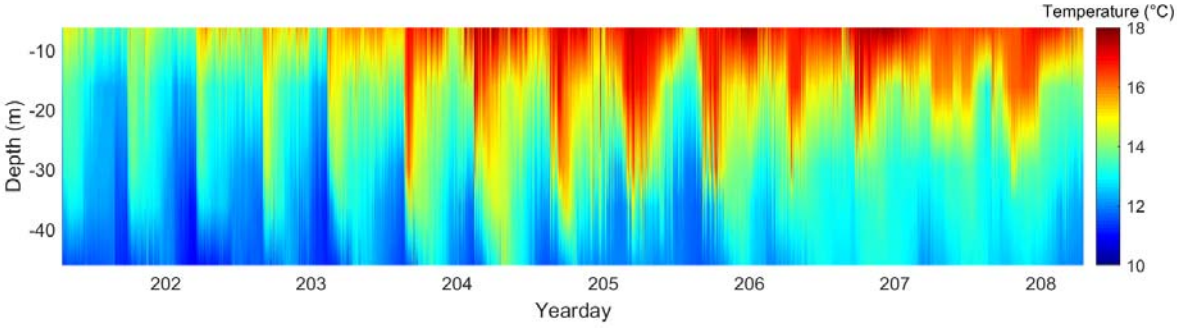

Figure 7g. Temperature Plot—Week 7.

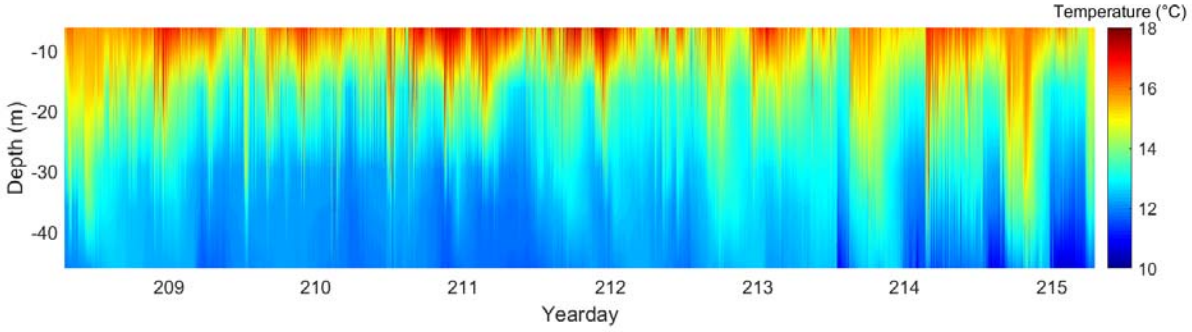

Figure 7h. Temperature Plot—Week 8, First 3 Days.

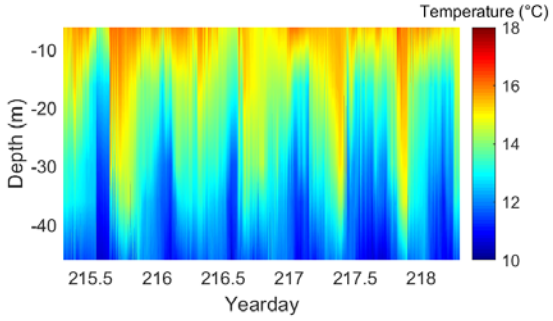

B. INTERNAL TIDES

From these plots, it was observed that there was great variability in internal wave activity, ranging from internal waves with small temperature difference (e.g., yeardays 174–177), to internal waves with large temperature difference (e.g., yeardays 204–208). The internal waves were observed to have two oscillations per day, matching the semidiurnal tidal frequency. Hence, it can be concluded that internal waves in this region were largely due to tidal forcing.

C. SOLITONS

Figure 8 shows the number of soliton occurrences per day. Great variability in the daily occurrence of solitons was also observed, ranging from no solitons during yeardays 174 and 178 to 37 solitons during yearday 210.

Figure 8. Daily Occurrence Rate of Solitons. Source: Colosi et al. (2016).

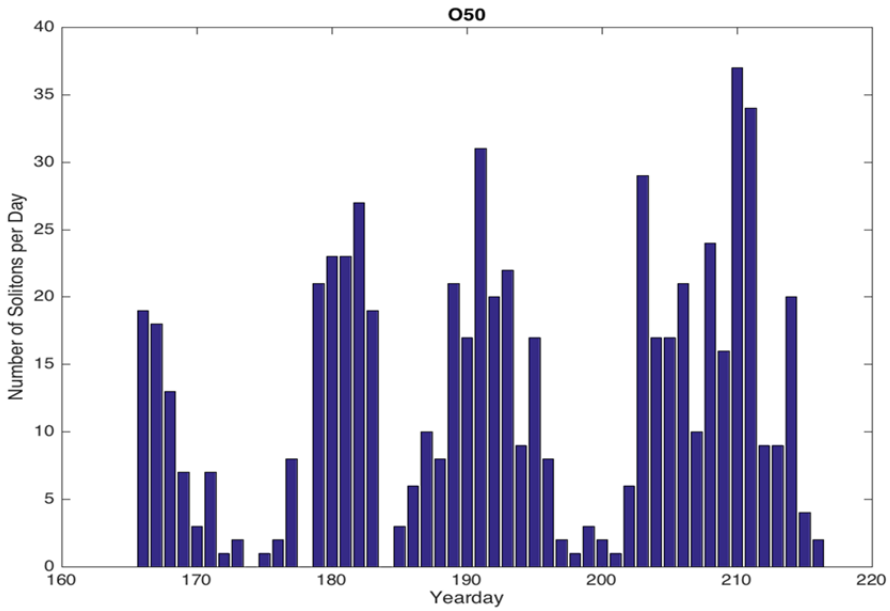

D. INTERNAL WAVE PERIOD, PROPAGATION SPEED, AND DIRECTION

Cross-correlation of temperature-strings in the experiment area (Colosi et al. 2016) showed that the internal waves propagated west to east at an average speed of 0.25 m/s (Figure 9, top), and at an average bearing of 80° with respect to true north (Figure 9, bottom). For ease of illustration, a purely eastward propagation of internal waves would be assumed for the study, as this is a general analysis of how internal waves affect sound propagation and is not tied to a specific bathymetry.

Figure 9. Speed of Internal Wave Propagation (top) and Direction of Internal Wave Propagation (bottom). Source: Colosi et al. (2016).

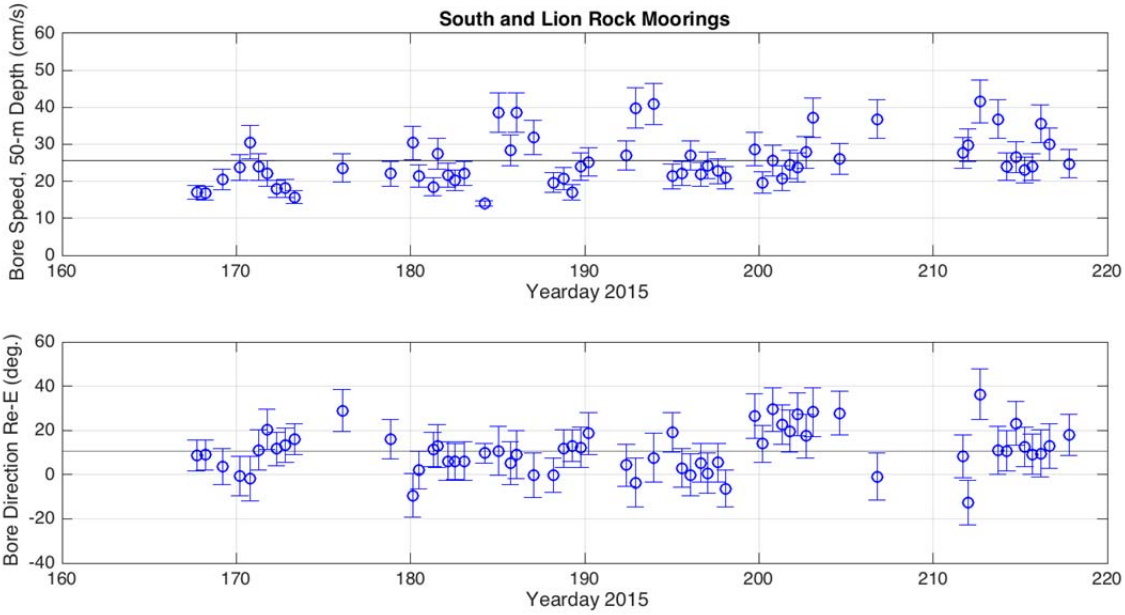

Internal tides in shallow waters are also called tidal bores, or simply bores. The angles used in the "Bore Direction" plot are with respect to east, and positive angles are anti-clockwise from east.

E. INTERNAL WAVE FRONTS IN THE EXPERIMENT AREA

The internal waves will be assumed to have a plane wave structure as they propagate eastward. This implies that sound waves that travel eastward or westward will cut across the internal wave fronts (red arrow of Figure 10); hence, a range-dependent SSP was used to simulate the behaviors of these sound waves. As for the sound waves that travel northward or southward, they will travel in-parallel or along the internal wave fronts (green arrow of Figure 10); hence, a range-independent sound speed profile was used to simulate the propagation behavior of these sound waves.

Figure 10. Sound Propagation Along and Across Internal Wave Fronts in the Experiment Area (figure not drawn to scale).

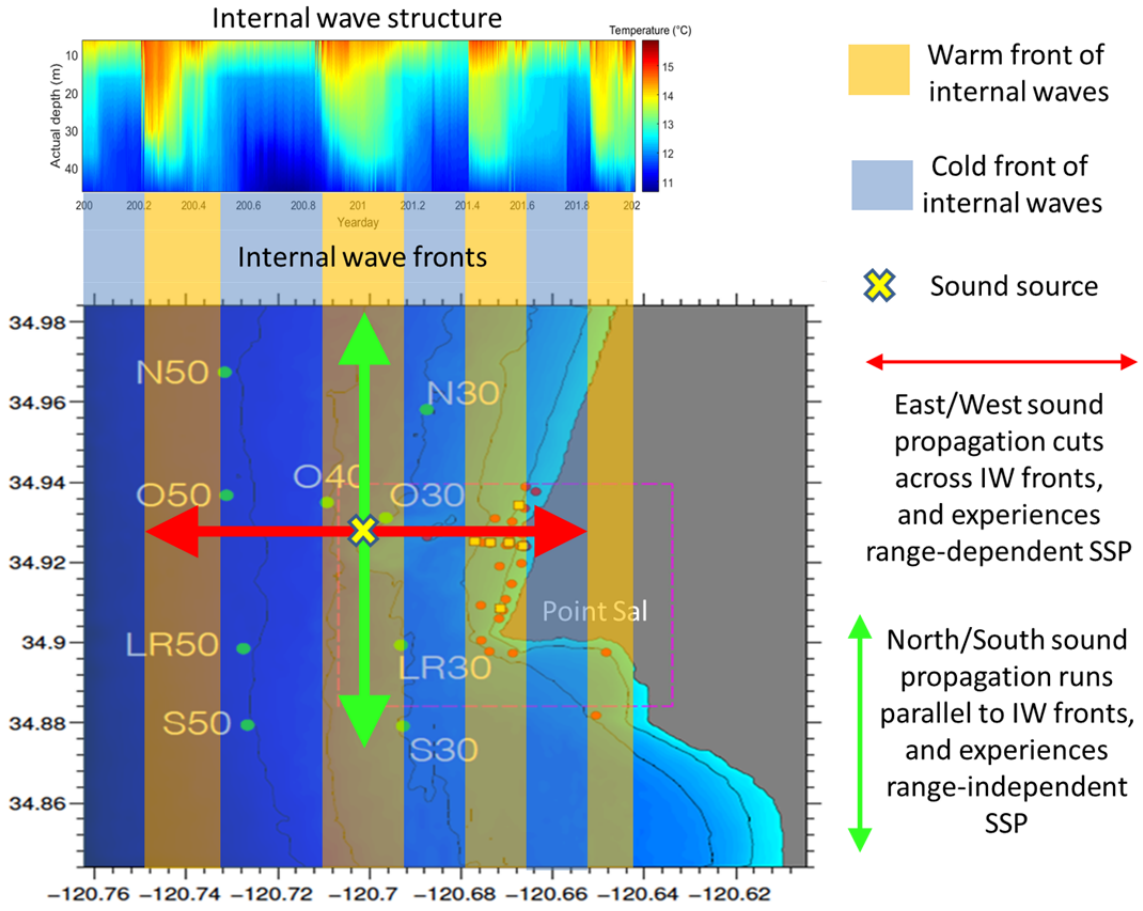

Assuming that the internal waves propagate eastward and have a plane wave structure, easterly/westerly sound propagation will cut across internal wave fronts (red arrow) and experience range-dependent sound propagation, while northerly/southerly sound propagation will run along internal wave fronts (green arrow) and experience range-independent sound propagation

F. TRANSLATING WATER TEMPERATURE TO SOUND SPEED

For the translation of temperature, depth, and salinity into sound speed, the nine-term Mackenzie equation was used (Mackenzie 1981), where sound speed (c) is a function of temperature (T) in degrees Celsius, salinity (S) in psu, and depth (D) in meters.

For the nine-term Mackenzie equation:

$$c(D,S,T) = 1448.96 + 4.591T - 5.304\,x\,10^{-2}T^2 + 2.374\,x\,10^{-4}T^3 + 1.340\,(S-35) + 1.630\,x\,10^{-2}D + 1.675\,x\,10^{-7}D^2 - 1.025\,x\,10^{-2}T(S-35) - 7.139\,x\,10^{-13}TD^3 \quad ,$$

the range of the equation validity is temperature: 2 to 30°C; salinity: 25 to 40 psu; depth: 0 to 8000 m.

From the Mackenzie equation, it can be seen that in shallow waters, changes in temperature are the primary cause of sound speed changes, while sound speed changes due to salinity changes are small in the experiment area as there was no introduction of fresh water into the region. An average salinity of 34.44 psu was used for the simulation runs.

Translation of wave measurements in time into distance traveled could be obtained by multiplying measurement time with internal wave propagation speed of 0.25 m/s. For semidiurnal internal tides (approximately 12 hours apart crest-to-crest), this translates to about 10.8 km between the crests of the internal tides. Over two days, the internal waves will propagate 43.2 km.

With the translation of internal wave measurements in time to physical distance, and the Mackenzie equation to get the SSP, there were sufficient data to generate a range-dependent sound speed profile to analyze the effects of internal waves on sound propagation.

An example of translating temperature readings into a range-dependent SSP is shown in Figure 11 for the two-day period of yeardays 200–202. The temperature as a function of time and depth plot of this particular period is as shown in the top plot of Figure 11. From this data, a range-dependent SSP (with depth adjustments to facilitate BELLHOP analysis) was derived, as shown in the bottom of Figure 11. For the x-axis, the time measurements were converted to range based on the internal wave propagation speed, with 0 km at yearday 200, and yearday 202 converts to 43.2 km west of temperature string O50 (as the internal wave fronts at that location will reach temperature string O50 two days later with an eastward propagation). Such range-dependent SSPs

were fed into BELLHOP for simulations runs, to determine their effects on sound propagation.

Figure 11. Temperature as a Function of Time and Depth (top) Translated to a Range-Dependent Sound Speed Profile (bottom).

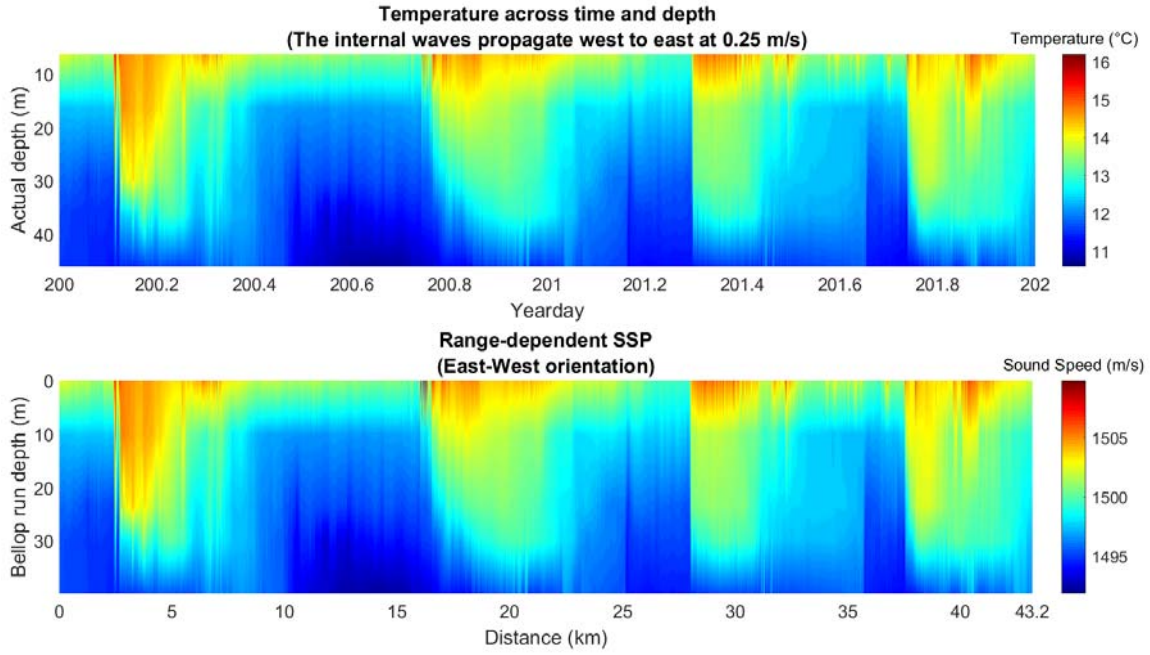

It should be noted that an increase in temperature leads to an increase in sound speed; hence, the structure of the temperature plot and the range-dependent SSP plot look similar. This means that the structure of the internal waves has a direct influence on sound speed and the shape of the internal waves can be seen from the range-dependent SSP.

V. BELLHOP—THE MODELING AND SIMULATION MODEL CHOSEN

A. RAY TRACING

A ray theory acoustic model called BELLHOP was used to ray trace the sound wave propagation path through the water. An example of a ray trace plot has been previously illustrated in Figure 3. The physics behind ray tracing is Snell's Law, which calculates the refraction of sound waves as they move horizontally through waters of different density and hence sound speeds. A depiction of Snell's Law is shown in Figure 12.

Figure 12. Depiction of Snell's Law. Adapted from Kapolka (2015).

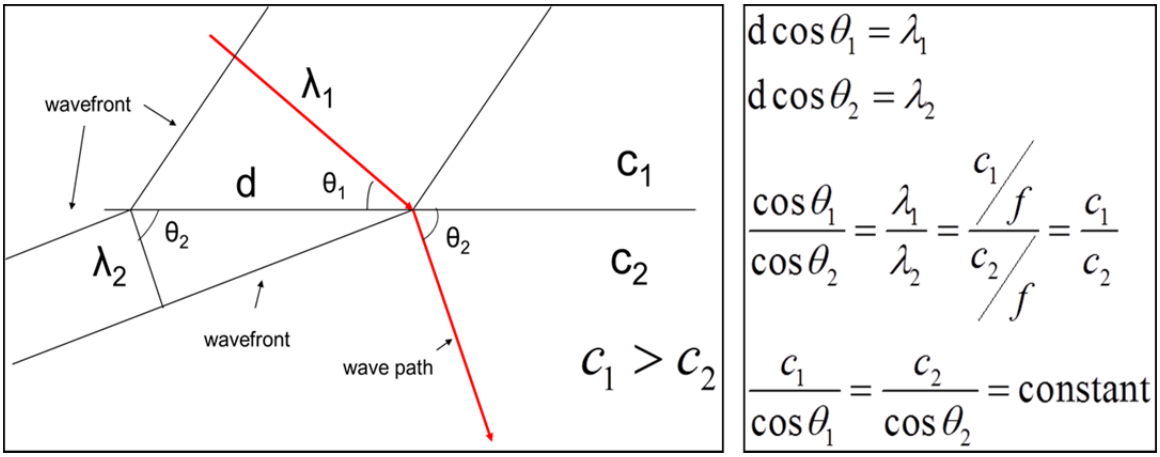

C_1, C_2: Sound speed of layer 1 and layer 2, respectively.

λ_1, λ_2: Wavelength of sound wave in layer 1 and layer 2.

θ_1, θ_2: Grazing angle, angle of sound "ray" with respect to the plane dividing the two mediums.

Given that $\frac{c_1}{\cos\theta_1} = \frac{c_2}{\cos\theta_2}$, sound waves will refract downward as sound speed decreases with depth, and will refract upward as sound speed increases with depth (see Figure 13).

Figure 13. Refraction of Sound Waves. Adapted from Kapolka (2015).

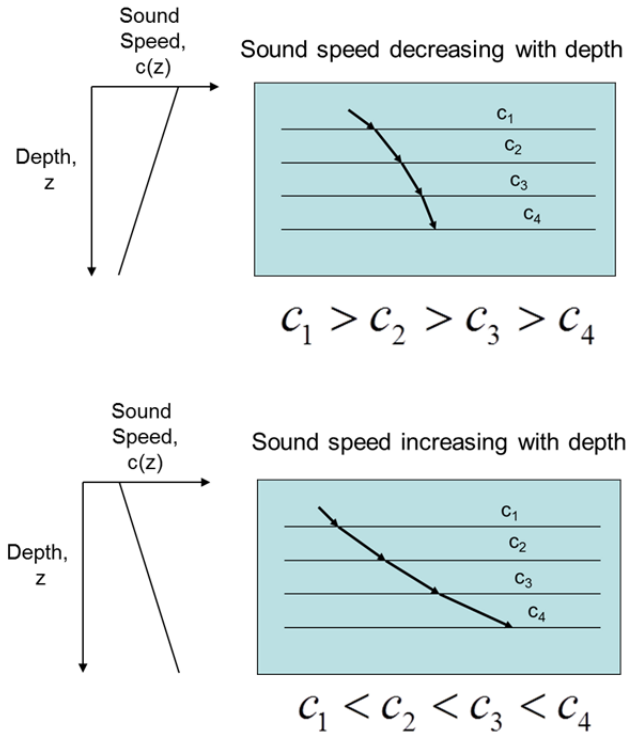

Top: Sound wave refracted downward as sound speed decreases with depth.

Bottom: Sound wave refracted upward as sound speed increases with depth.

C_1, C_2, C_3, C_4: Sound speed of the various layers.

To generate the transmission loss plots as seen in Figure 5, BELLHOP ray traces a large number of sound "rays" emanating from a sound source and then sums the intensity of the rays as they move downrange.

B. WHY BELLHOP RAY THEORY ACOUSTIC MODEL

A ray theory acoustic model was chosen as this study uses ray tracing of the sound waves to demonstrate how internal waves modulate their interactions with the seabed. The other reason was that a ray theory acoustic model could also support range-dependent SSPs (Etter 2013), which are required in this study as internal waves will cause the SSPs to vary with range.

C. BELLHOP'S ENVIRONMENTAL PARAMETERS

1. Adjustment of Actual Sea Depth to BELLHOP Model's Depth

As there were no temperature sensors at the sea surface and seabed for temperature string O50, a translational step was made to ensure compatibility with BELLHOP by treating the shallowest sensor as being at the top boundary of the water column and the deepest sensor as being at the bottom boundary of the water column in BELLHOP. This eliminates the need to extrapolate the temperature readings to the sea surface and the seabed.

The actual depth of the temperature sensors and their adjusted depth in BELLHOP are as listed in Table 2. The depth adjustment was done by treating the shallowest sensor depth (at 6.2 m) as the "surface sensor" (of 0 m) and adjusting all the sensor depths upward by 6.2 m, with the depth of the deepest sensor rounded to 40 m.

Table 2. Temperature String O50—Temperature Sensor Depths.

Actual sensor depth	Adjusted depth for BELLHOP run (by -6.2 m)
6.2 m	0.0 m
16.3 m	10.1 m
29.7 m	23.5 m
36.1 m	29.9 m
46.1 m	Rounded to 40.0 m

2. Flat Bathymetry and Smooth Sea Surface

To enable a general study of the effect of internal waves on sound propagation, a flat seabed and a smooth sea surface were used in the simulation runs, so as not to limit the applicability of the analysis to a specific location.

3. Sound Source Depth

The sound source was placed at a depth of 38 m for the simulation runs so that sound rays launched at small angles with respect to the horizontal plane would not be refracted downward too much before striking the seabed. This allows them to graze the seabed at a small angle, so that most of their energy will be reflected, thus enabling them to propagate farther, as is the case for many underwater applications.

D. MEASURES TO MAXIMIZE SIMULATION ACCURACY

1. Ray Trace Using a Frequency of 2 kHz

Etter (2013) states that the geometrical acoustics approximation made for the ray theory model, which assumes that sound speed does not change much over one wave length horizontally, limits the ray acoustics to higher frequency applications (as lower frequency sound waves have longer wave lengths).

Etter (2013) also gives a guideline for defining the frequency above which a ray acoustics model becomes suitable for use, in the following equation:

$$f > 10\frac{c}{\mathrm{H}},$$

where f is the frequency, H is the water depth, and c is the speed of sound. With a BELLHOP simulation depth of 40 m, and using an average sound speed of 1500 m/s, the formula resolves to f > 375 Hz. A frequency of 2 kHz, which is around the frequency range of a mid-frequency sonar, was used for the study and is well above the 375 Hz threshold.

2. Gaussian Beam Option

Ray trace models are unable to approximate the effects of caustics, which are regions of intense beam focusing. One method to mitigate this is Gaussian beam tracing. Porter and Bucker (1987) state that Gaussian beam tracing avoids the traditional ray trace artefact of infinite energy levels at caustics, and is attractive for high-frequency, range-

dependent applications. Hence, the Gaussian beam option in BELLHOP was used to increase the ray trace modeling accuracy.

3. Cubic Spline Fitting of the SSP Plot

The depth interval between sensors on temperature string O50 was 10 meters. Such a coarse depth resolution could cause inaccuracies in ray tracing if straight lines (linear interpolation) were used to join the data points. To overcome this, the cubic spline interpolation of the SSP was used in the BELLHOP runs, which replaced the linear approximation with a more realistic curved line for the SSP (see Figure 14).

Figure 14. Comparison between Straight Line Linear Approximation and Cubic Spline Interpolation of the Sound Speed Profile.

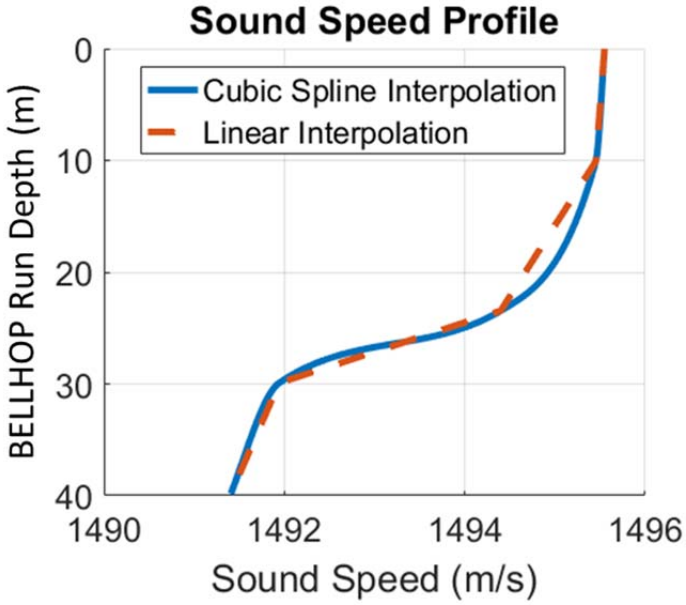

4. Incoherent Beam Option

The BELLHOP simulation runs were conducted using the "incoherent" beam option, which allows a smoothed transmission loss plot of the sound energy over range. A "coherent" beam option would have accounted for the phase of the sound waves and shown the constructive and destructive interferences of the signal over range as distinctive peaks and null in the transmission loss plot. The difference in transmission

loss between an incoherent and a coherent beam option is illustrated in Figure 15. The incoherent beam option was chosen as this study is focused on the effects of internal waves on sound propagation over longer ranges, and does not require an in-depth analysis of the effects of constructive and destructive interferences of the signal over short distances of a few wave lengths.

Figure 15. Incoherent Transmission Loss (top), Coherent Transmission Loss (bottom).

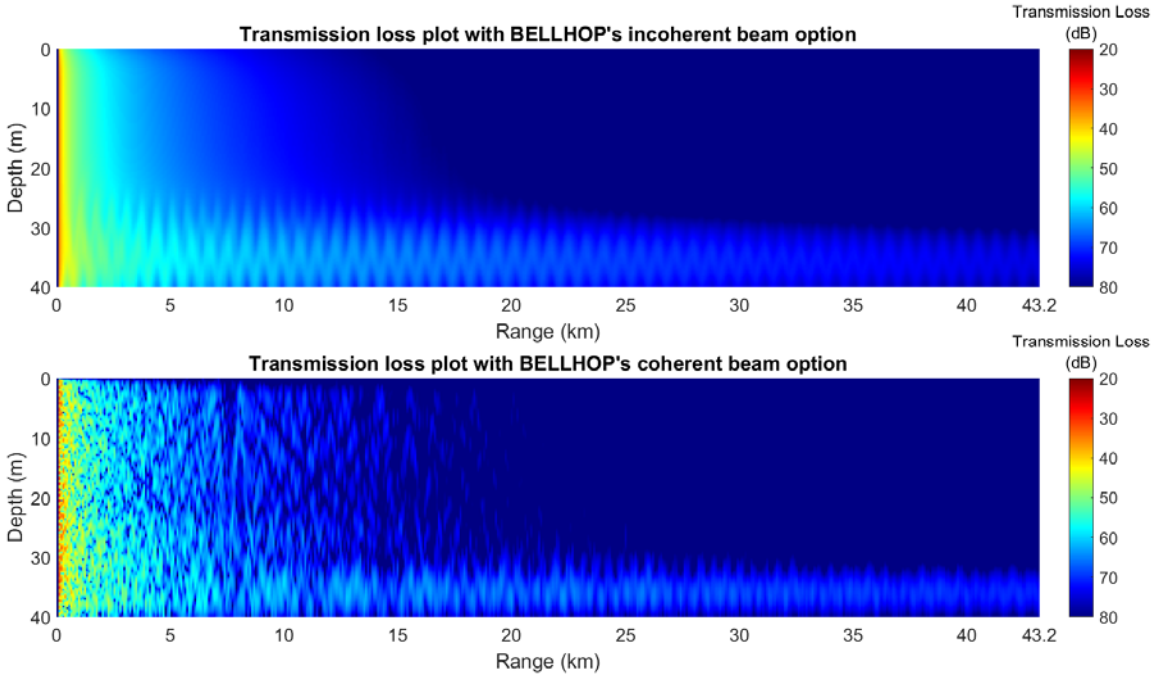

VI. TYPES OF ANALYSIS AND THEIR CONSIDERATIONS

A. TIME PERIODS CHOSEN FOR ANALYSIS

Five time periods with distinct internal wave characteristics were chosen from the experiment data for the BELLHOP simulation runs (Table 3). The first was the period at yeardays 175–177, which was a period of well-defined internal tides with few solitons. The difference between the surface and bottom water temperature in this period was small at 2.5°C.

The second period was at yeardays 205–207, which was also a period of well-defined internal tides, but with many solitons. The surface and bottom water temperature difference in this period was large at 7°C.

The third period was at yeardays 210–212, which was a period of weak internal tides but with a large number of soliton occurrences and a surface and bottom water temperature difference of 6°C.

The fourth period, at yeardays 200.6–202.9, had well-defined internal tides but few solitons and a surface and bottom water temperature difference of 5°C. Two simulation runs were conducted for period 4, one with the sound source in the middle of the cold front of an internal tide (yearday 200.6, period 4a of Table 3), the other with the sound source in the middle of the warm front of an internal tide (yearday 200.9, period 4b of Table 3).

The fifth period was at approximately yearday 174.22, which was at the warm and cold interface of a steep tidal bore. Two simulation runs were conducted at data points that were 5 minutes or 75 m apart, with one run at the warm front of the tidal bore and the other run at the cold front of the tidal bore.

Table 3. Internal Wave Characteristics of the Selected Time Periods for Analysis.

Period No.	Yearday	Internal tide	Solitons	Temperature across time and depth
1	175–177	-Well-defined -Small temperature difference (2.5°C)	Few	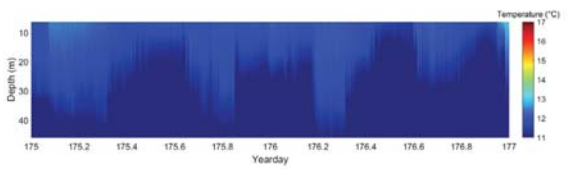
2	205–207	-Well-defined -Large temperature difference (7°C)	Many	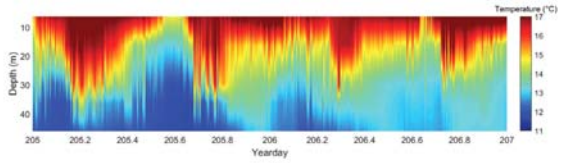
3	210–212	-Weak -Large temperature difference (6°C)	Many	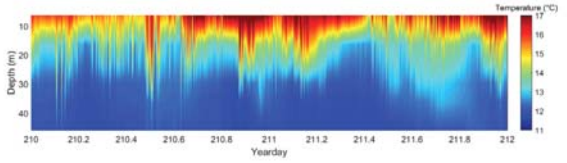
4a	200.6–202.6 Cold front of IW	-Well-defined -Fairly large temperature difference (5°C)	Few	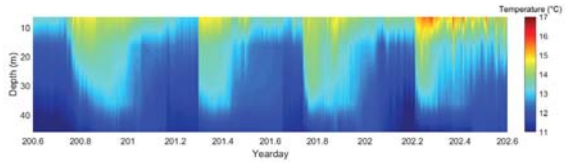 Starts at the cold front of an internal tide
4b	200.9–202.9 Warm front of IW	Same as period 4b	Same as period 4b	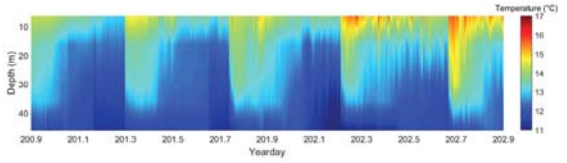 Starts at the warm front of an internal tide
5	174.2–176.2 Edge of tidal bore	Same as period 1	Same as period 1	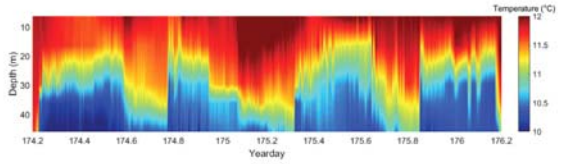 Two runs at 5 minutes or 75 m part were conducted; one starts at the cold front of the steep tidal bore, the other starts at the warm front of the tidal bore. (Note: This plot has a different color scale from the previous plots to accentuate the temperature differences)

B. BELLHOP PLOTS USED FOR ANALYSIS

Transmission loss plots are generated using range-independent and range-dependent SSPs, so that a quantitative comparison could be made on how much internal waves affect sound propagation (range-dependent SSP) as compared to a model that does not account for internal waves (range-independent SSP). An example of a range-independent and range-dependent sound speed profile is shown in Figure 16.

Figure 16. Range-Independent SSP (top), Range-Dependent SSP (bottom).

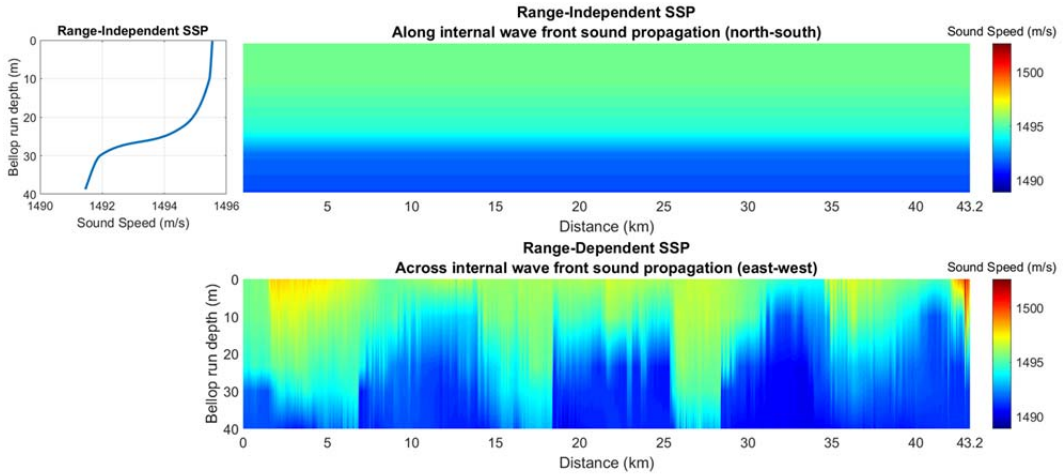

It has been mentioned that a range-independent SSP would be more appropriate for simulating along internal wave front sound propagation (northward/southward in the experiment area), while the range-dependent SSP would be more appropriate for simulating across internal wave front sound propagation (eastward/westward in the experiment area).

Two types of transmission plots are generated; the first is the "traditional" transmission loss plot that has been shown in Figure 5, which uses a gradual color scheme to show the gradual loss of signal strength over range. Such plots allow the sound loss "structure" to be seen.

The second type of transmission loss plot is the 70 dB transmission range plot, an example of which is shown in Figure 17. Such plots allow a quantitative assessment of

the range a sound signal can reach before its transmission loss exceeds 70 dB. Referring to Figure 18, yellow shows the region where transmission loss is less than 70 dB, while dark blue shows the region where transmission loss is more than 70 dB. A transmission loss of 70 dB was chosen as the cut-off value in this study as it allows the display area of the plot to be maximized, which for the case of a rocky bottom of Figure 18, the 70 dB transmission loss is at 40 km, which is almost to the end of the plot. For this study, the 70 dB transmission ranges are measured from the source range (0 km) to the maximum range that the 70 dB contour reaches.

Figure 17. Example of a 70 dB Transmission Range Plot.

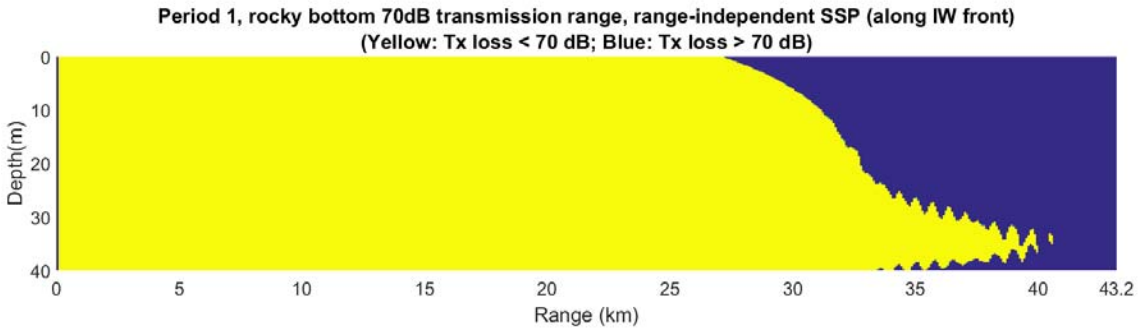

VII. RESULTS OF MODELING AND SIMULATION RUNS

A. PERIOD 1: INTERNAL TIDES WITH SMALL TEMPERATURE DIFFERENCE, FEW SOLITONS

The first period chosen for analysis (yeardays 175–177) was characterized by well-defined internal tides, with a small temperature difference of 2.5°C (from 10 to 12.5°C) between the bottom and the surface of the water, and few solitons (fewer than 5 solitons a day, see Figure 8).

The sound speed profile ranged from approximately 1489 m/s to 1498 m/s. The range-independent sound speed profile and range-dependent sound speed profile are shown in Figure 18, and the SSP at 0 km is at yearday 175. It can be seen from the range-independent sound speed profile (Figure 19, top) that a bottom layer exists from 30–40 m depth, and this should serve to give an extended transmission range in the bottom layer due to downward refraction trapping sound energy in the lower water column.

The transmission loss plots for the three types of seabed, with a range-independent SSP and range-dependent SSP, are shown in Figure 19. The 70 dB transmission range plots are shown in Figure 20. The sound source depth for all these plots is 38 m.

Across all bottom types, the modeling runs that accounted for internal waves gave a reduced transmission range compared to a modeling run that does not factor the effects of internal waves. For the rocky seabed, the 70 dB transmission range dropped from 40.0 km for along internal wave front propagation to 21.5 km for across internal wave front propagation. For the sandy seabed, the 70 dB transmission range dropped from 27.3 km to 6.2 km, while for the muddy seabed, the 70 dB transmission range dropped from 26.5 km to 2.5 km. Hence, it can be seen that for a small temperature difference between the seabed and sea surface, and with a bottom layer, factoring the effects of internal waves resulted in significant acoustics range reduction compared to a model that does not account for internal waves.

Figure 18. Period 1—Range-Independent SSP (top), Range-Dependent SSP (bottom) 0 km at Yearday 175.

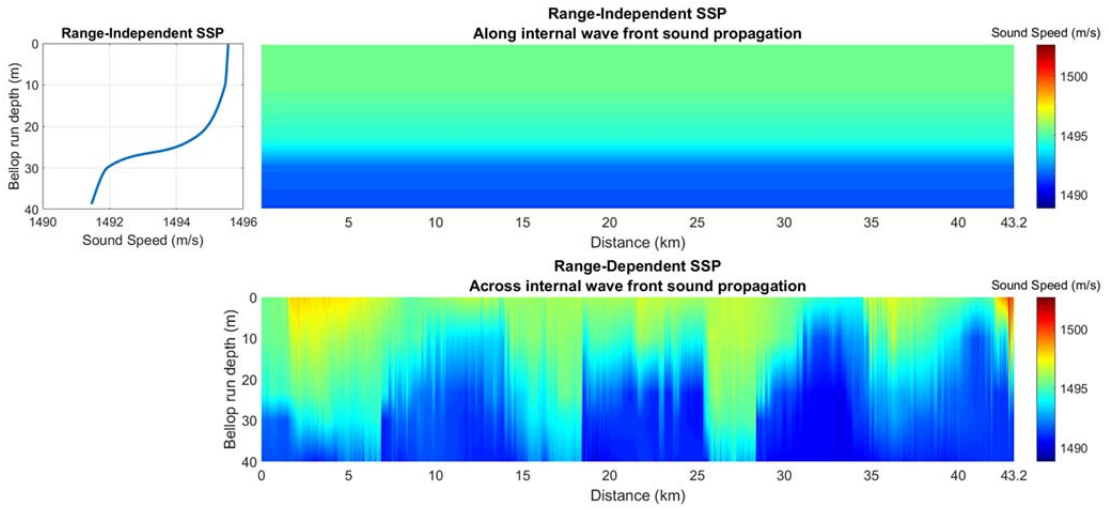

Figure 19. Period 1—70 dB Transmission Range for a Rocky, Sandy, and Muddy Seabed. (Figures 19a–c).

Figure 19a. Period 1—Rocky Bottom Transmission Loss through Range-Independent SSP and Range-Dependent SSP.

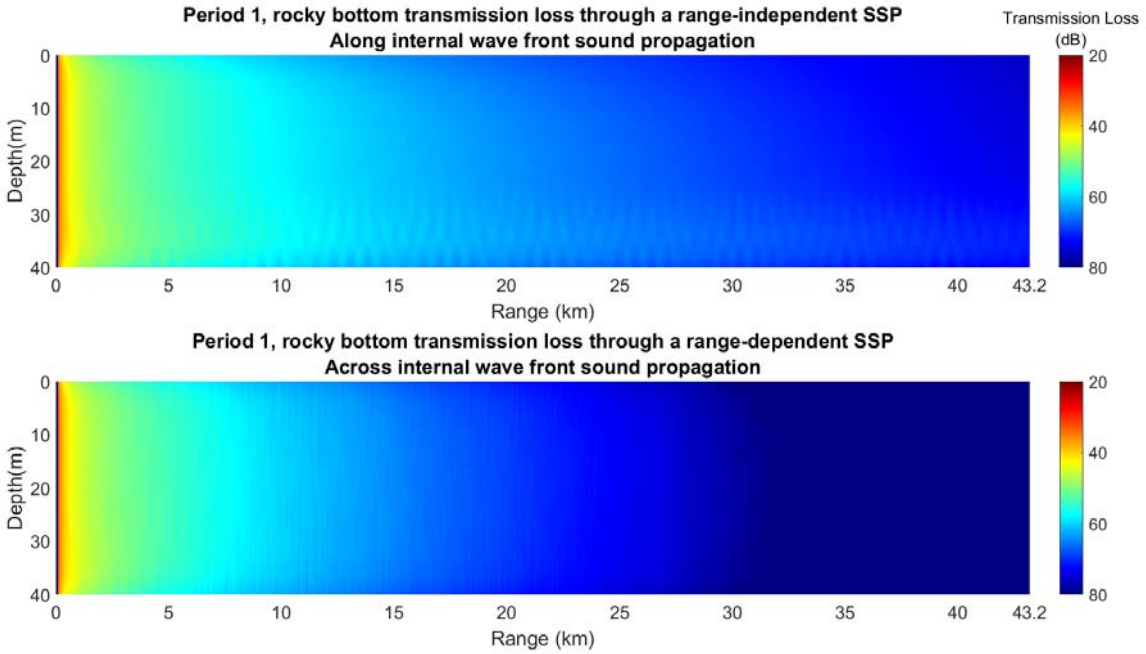

Figure 19b. Period 1—Sandy Bottom Transmission Loss through Range-Independent SSP and Range-Dependent SSP.

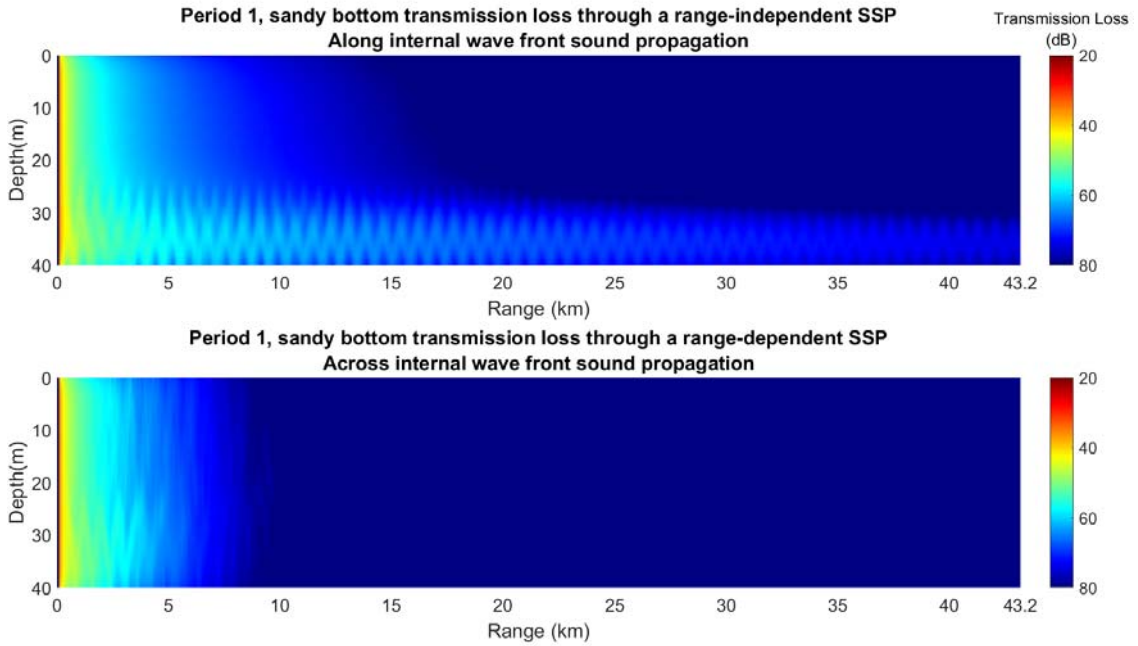

Figure 19c. Period 1—Muddy Bottom Transmission Loss through Range-Independent SSP and Range-Dependent SSP.

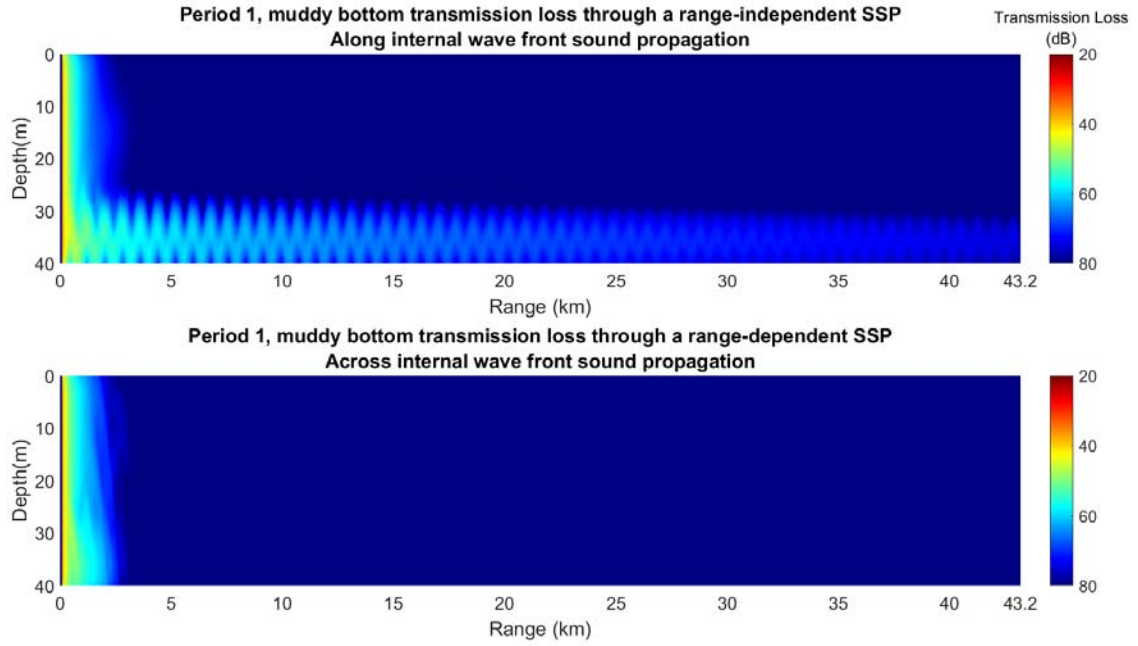

Figure 20. Period 1—70 dB Transmission Range for a Rocky, Sandy, and Muddy Seabed. (Figures 20a–c).

Figure 20a. Period 1—Rocky Bottom 70 dB Transmission Range for a Range-Independent SSP and a Range-Dependent SSP.

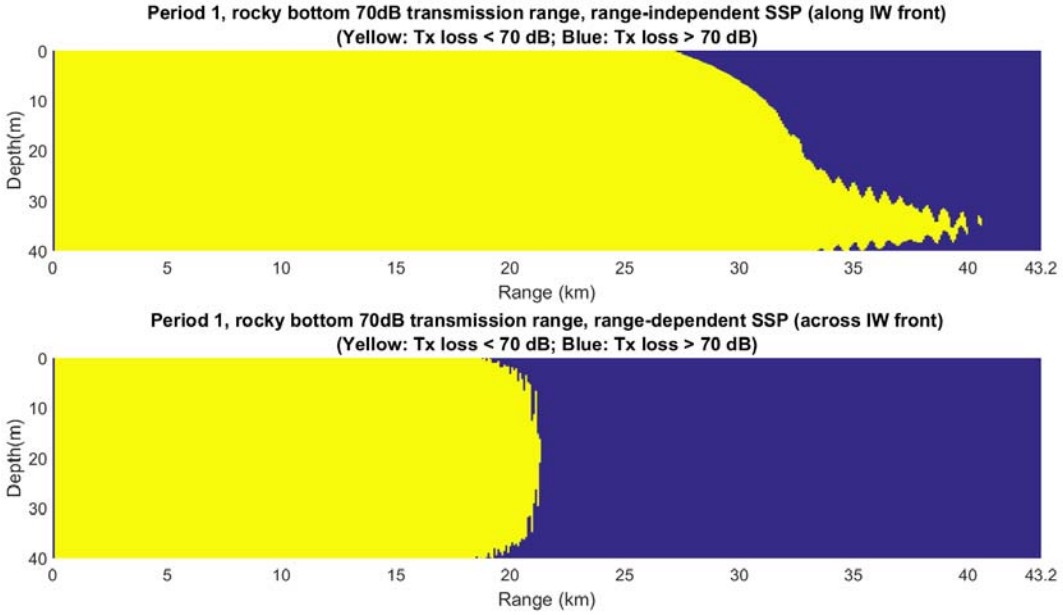

Figure 20b. Period 1—Muddy Bottom 70 dB Transmission Range for a Range-Independent SSP and a Range-Dependent SSP.

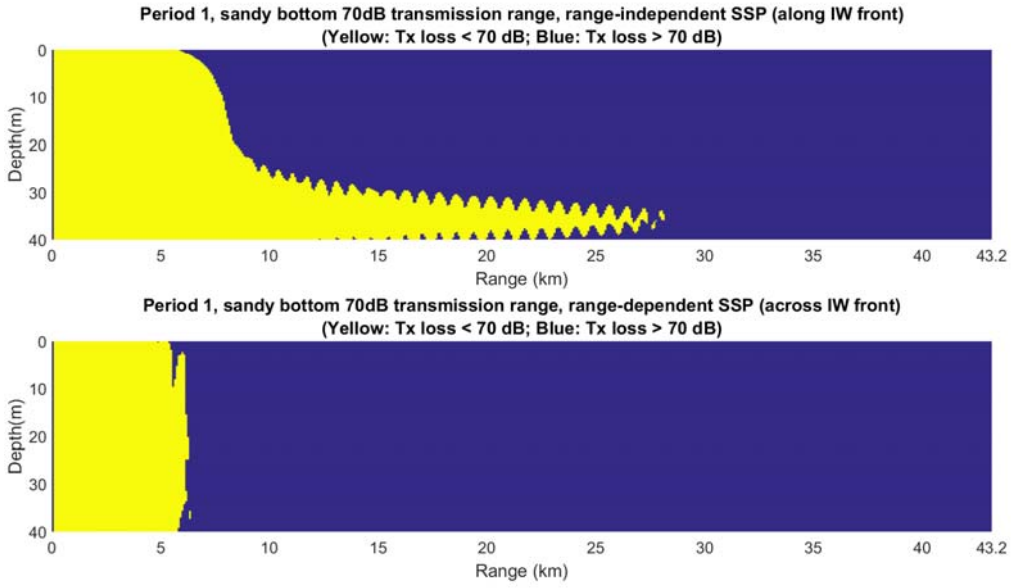

Figure 20c. Period 1—Muddy Bottom 70 dB Transmission Range for a Range-Independent SSP and a Range-Dependent SSP.

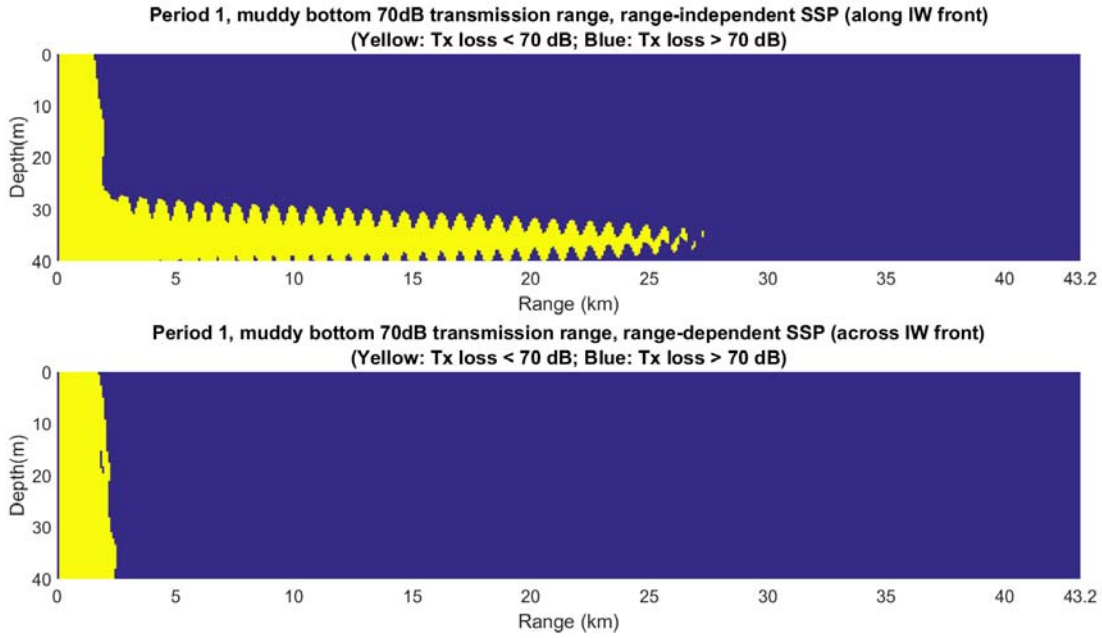

B. PERIOD 2: INTERNAL TIDES WITH LARGE TEMPERATURE DIFFERENCE, MANY SOLITONS

This period (yeardays 205–207) was characterized by well-defined internal tides, with a large temperature difference of 7°C (from 11 to 18°C) between the bottom and the surface of the water, and many solitons (more than 15 solitons per day, see Figure 8). The sound speed profile ranged from approximately 1494 m/s to 1515 m/s. The range-independent sound speed profile and range-dependent sound speed profile are shown in Figure 21, and the SSP at 0 km is centered at yearday 205. The transmission loss plots for the three types of seabed are shown in Figure 22, while the 70 dB transmission range plots are shown in Figure 23.

Similar to period 1, factoring for internal waves in the model causes more attenuation compared to a modeling run without internal waves. For the rocky seabed, the 70 dB transmission range dropped from 37.5 km to 18.3 km when the effects of internal waves were accounted for. For the sandy seabed, the 70 dB transmission range dropped

from 12.2 km to 6.5 km, while for the muddy seabed, the 70 dB transmission range actually increased from 1.8 km to 2.5 km.

Figure 21. Period 2—Range-Independent SSP (top), Range-Dependent SSP (bottom) 0 km at Yearday 205.

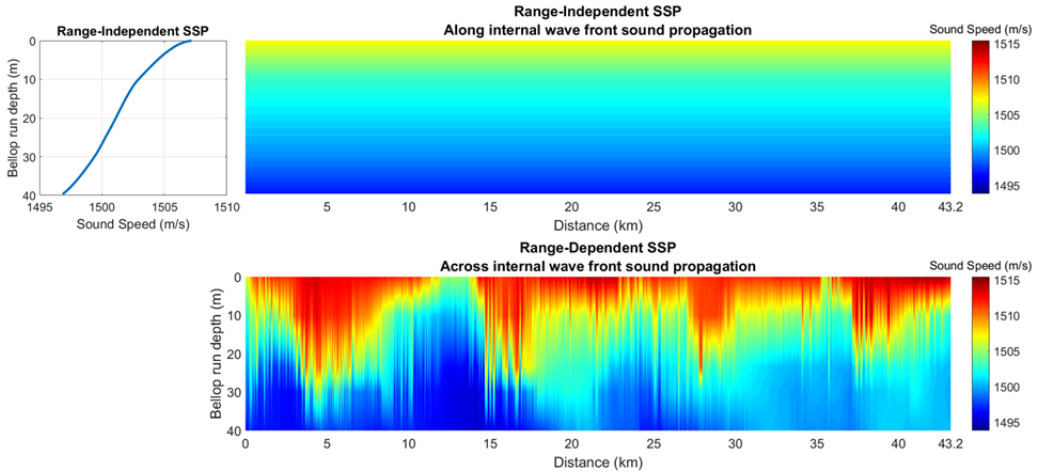

Figure 22. Period 2—Transmission Loss for a Rocky, Sandy, and Muddy Seabed. (Figures 22a–c).

Figure 22a. Period 2—Rocky Bottom Transmission Loss through Range-Independent SSP and Range-Dependent SSP.

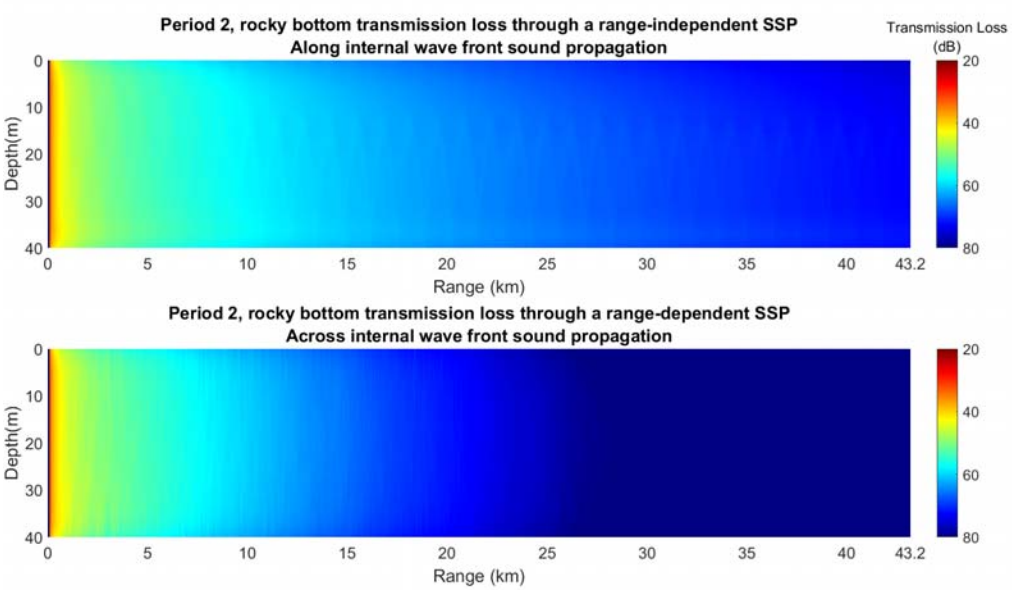

Figure 22b. Period 2—Sandy Bottom Transmission Loss through Range-Independent SSP and Range-Dependent SSP.

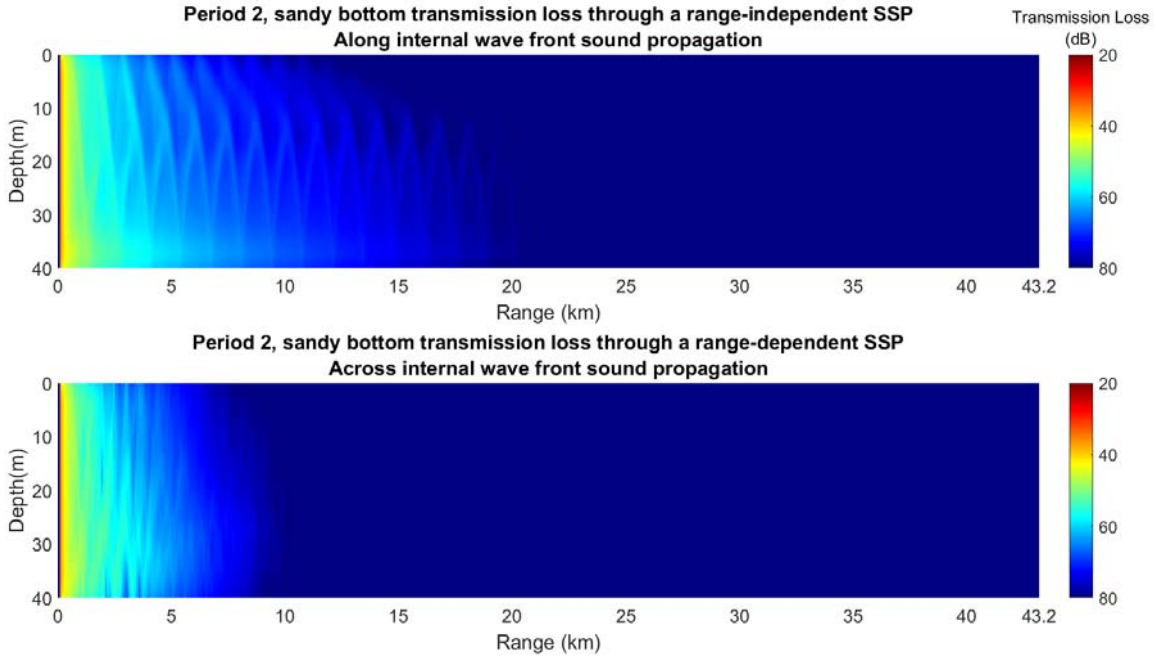

Figure 22c. Period 2—Muddy Bottom Transmission Loss through Range-Independent SSP and Range-Dependent SSP.

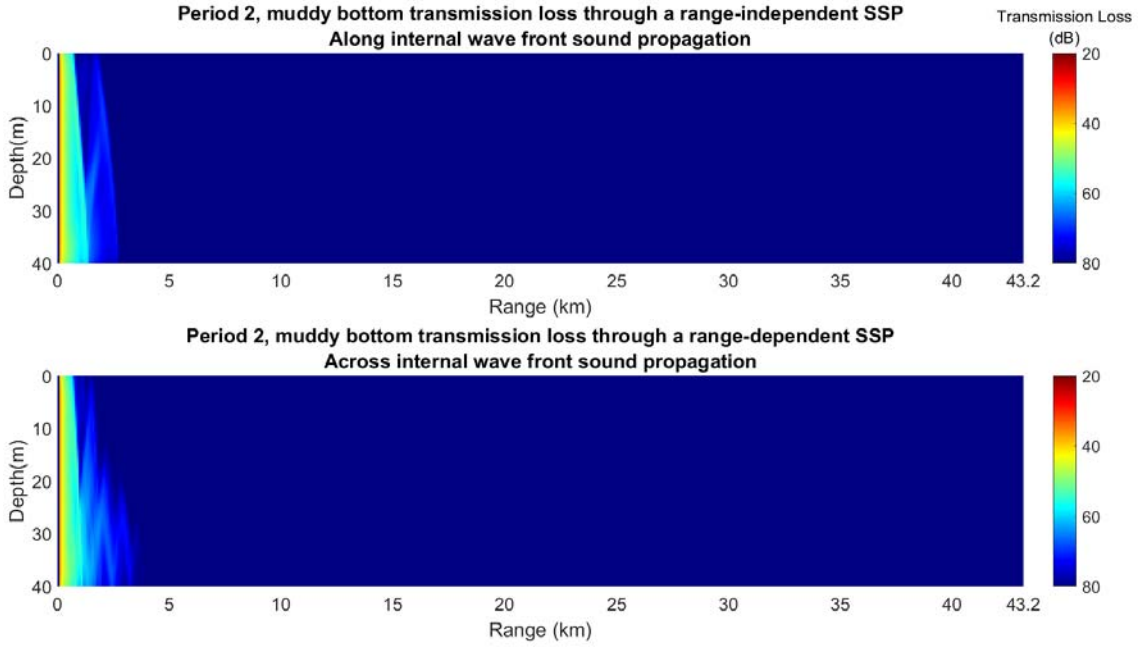

Figure 23. Period 2—70 dB Transmission Range for a Rocky, Sandy, and Muddy Seabed. (Figures 23a–c).

Figure 23a. Period 2—Rocky Bottom 70 dB Transmission Range for a Range-Independent SSP and a Range-Dependent SSP.

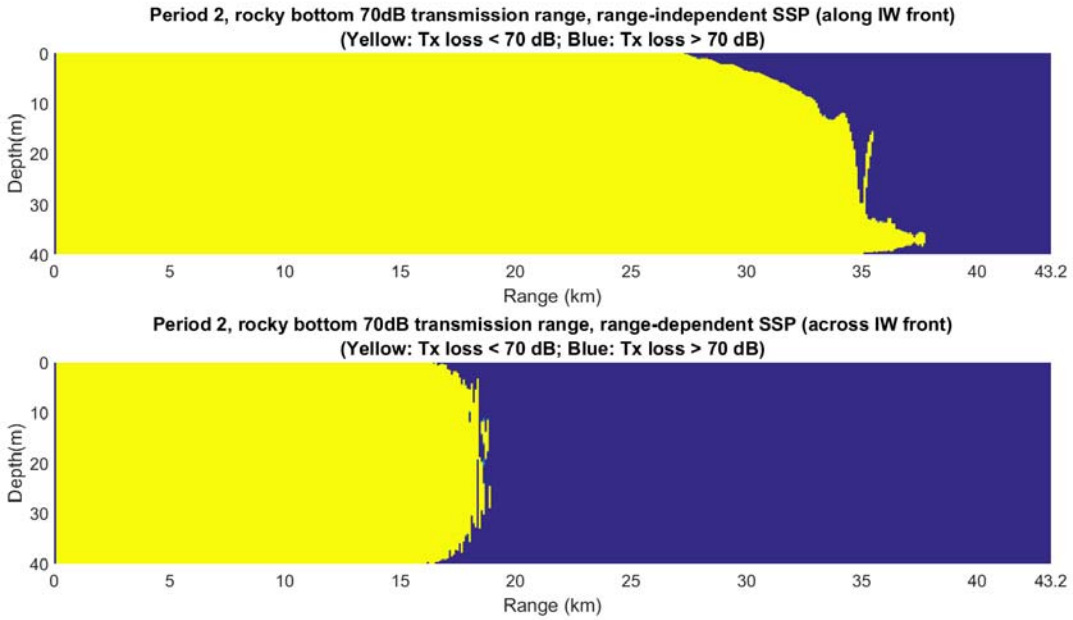

Figure 23b. Period 2—Sandy Bottom 70 dB Transmission Range for a Range-Independent SSP and a Range-Dependent SSP.

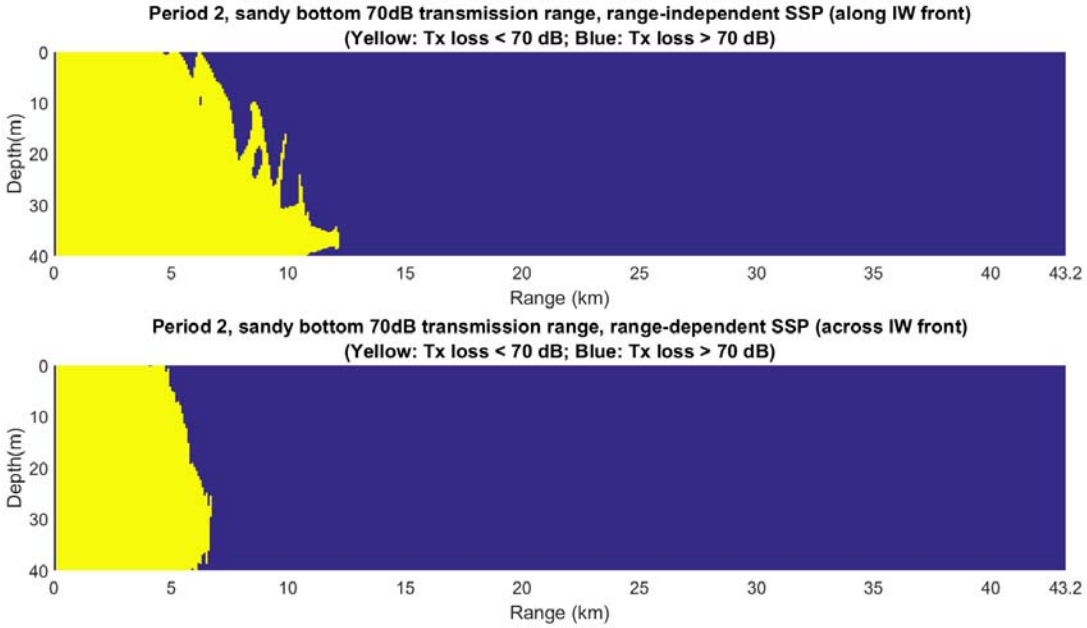

Figure 23c. Period 2—Muddy Bottom 70 dB Transmission Range for a Range-Independent SSP and a Range-Dependent SSP.

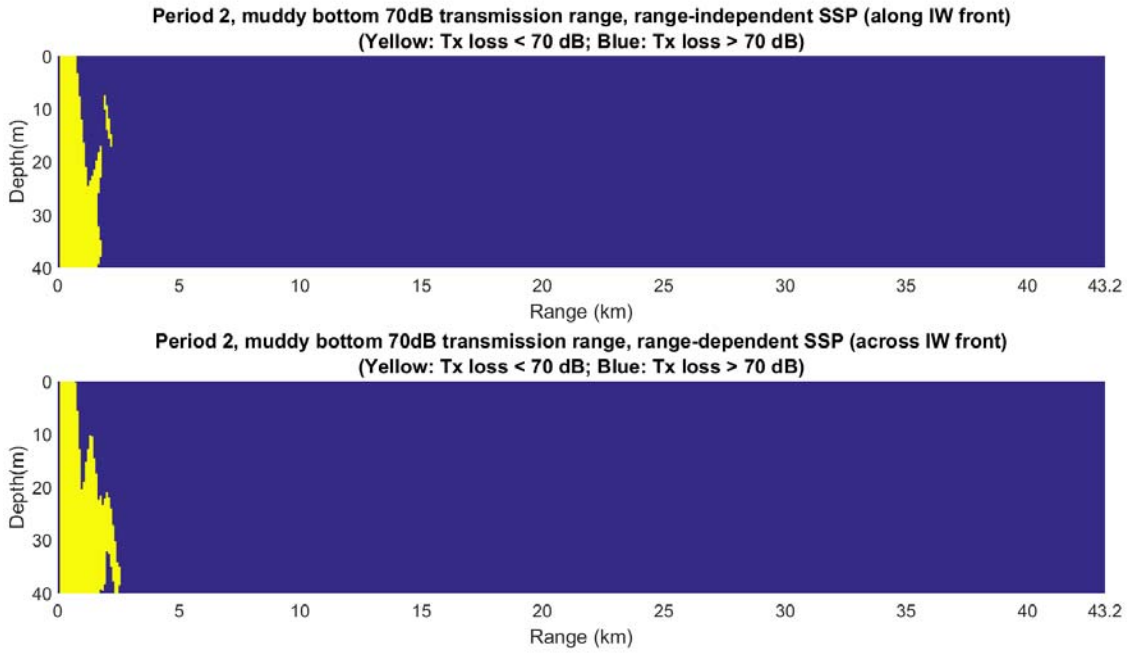

C. PERIOD 3: WEAK INTERNAL TIDES, MANY SOLITONS

This period (yeardays 210–212) was characterized by weak internal tides and many solitons (more than 15 solitons per day, see Figure 8). The water temperature difference was strong at 6°C (from 11.5 to 17.5°C) between the bottom and the surface of the water. The sound speed profile ranged from approximately 1495 m/s to 1514 m/s. The range-independent sound speed profile and range-dependent sound speed profile are shown in Figure 24, and the SSP at 0 km is at yearday 210. The transmission loss plots for the three types of seabed are shown in Figure 25, while the 70 dB transmission range plots are shown in Figure 26.

The simulation showed that even with internal waves only in the form of solitons, they still caused a range reduction as compared to a simulation that does not account for internal waves. For a rocky bottom, the 70 dB transmission range was reduced from 36.8 km for along internal wave front propagation to 18.5 km for across internal wave front propagation. For a sandy bottom, the range was reduced from 17.2 km to 9.5 km. For a muddy bottom, the range was reduced from 7.5 km to 3.7 km.

Figure 24. Period 3—Range-Independent SSP (top), Range-Dependent SSP (bottom) 0 km at Yearday 210.

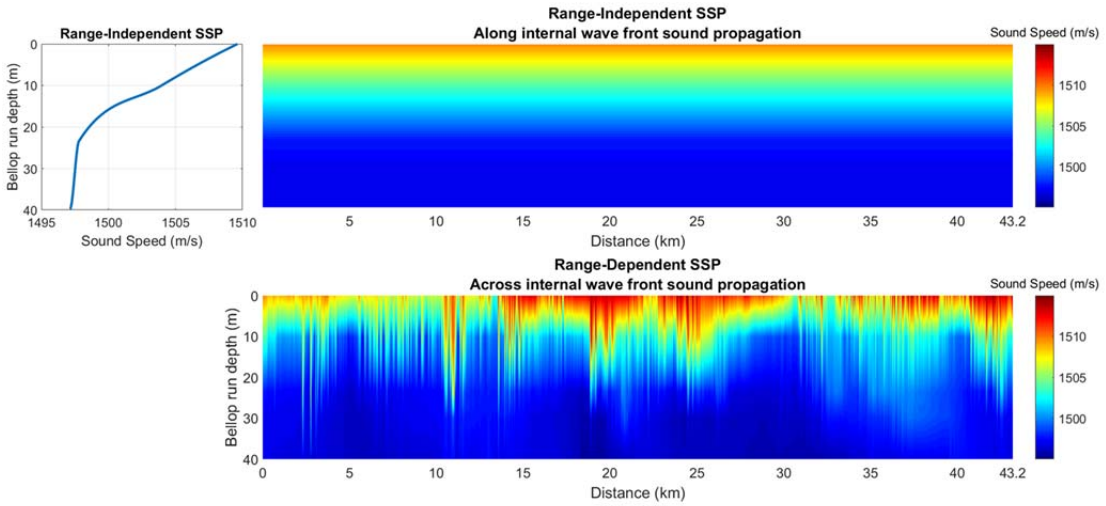

Figure 25. Period 3—Transmission Loss for a Rocky, Sandy, and Muddy Seabed. (Figures 25a–c).

Figure 25a. Period 3—Rocky Bottom Transmission Loss through Range-Independent SSP and Range-Dependent SSP.

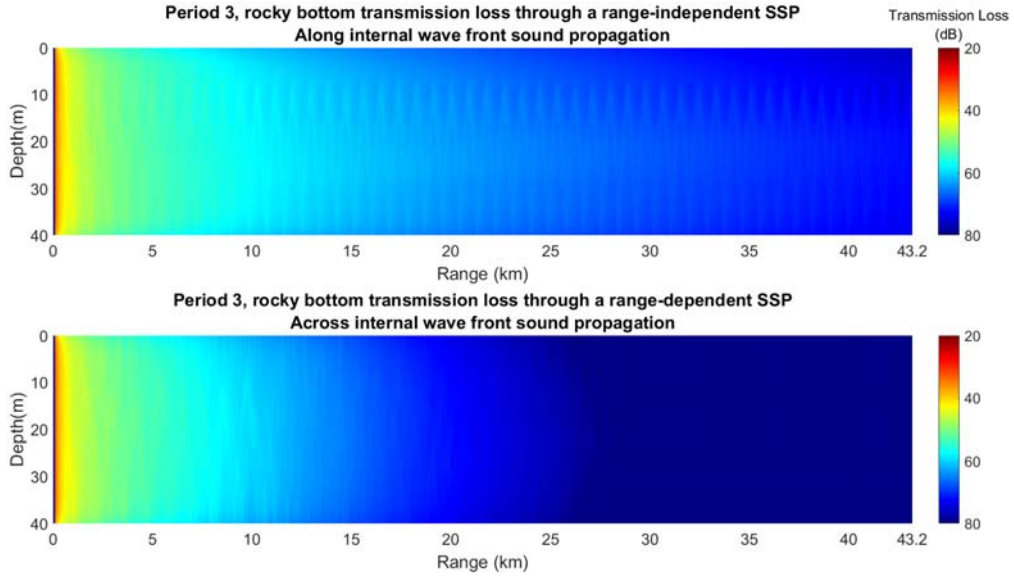

Figure 25b. Period 3—Sandy Bottom Transmission Loss through Range-Independent SSP and Range-Dependent SSP.

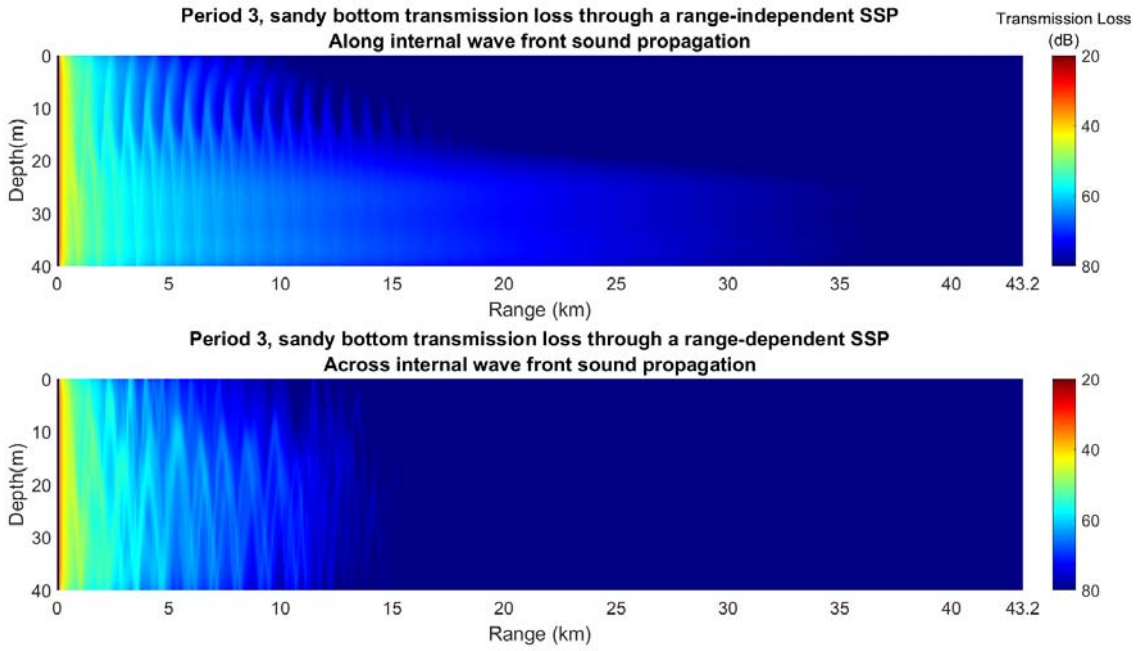

Figure 25c. Period 3—Muddy Bottom Transmission Loss through Range-Independent SSP and Range-Dependent SSP.

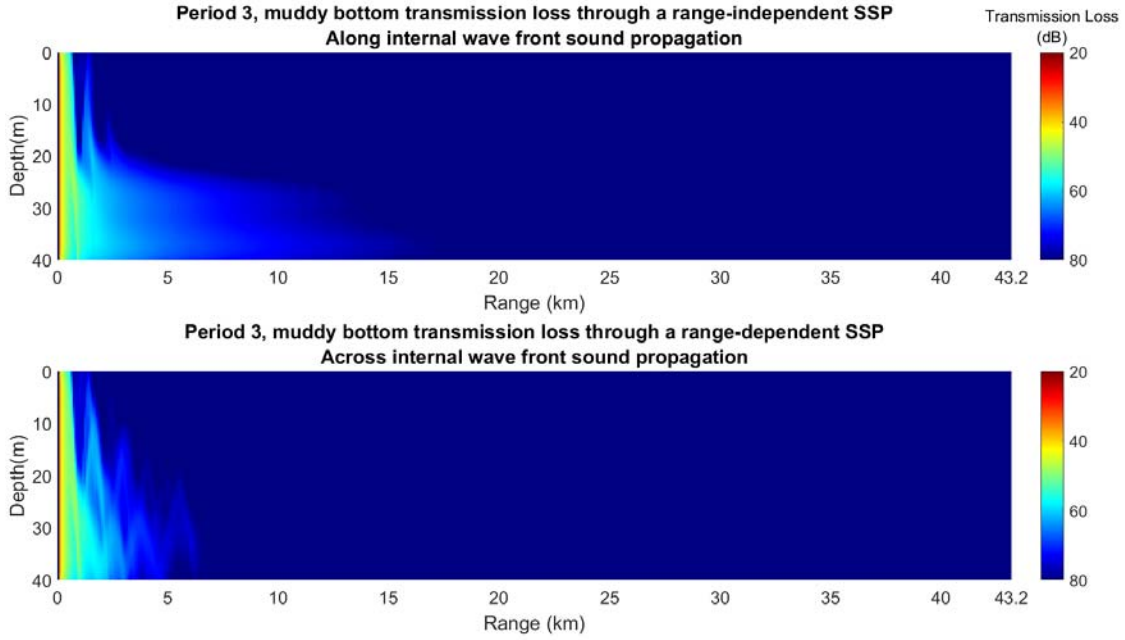

Figure 26. Period 3—70 dB Transmission Range for a Rocky, Sandy, and Muddy Seabed. (Figures 26a–c).

Figure 26a. Period 3—Rocky Bottom 70 dB Transmission Range for a Range-Independent SSP and a Range-Dependent SSP.

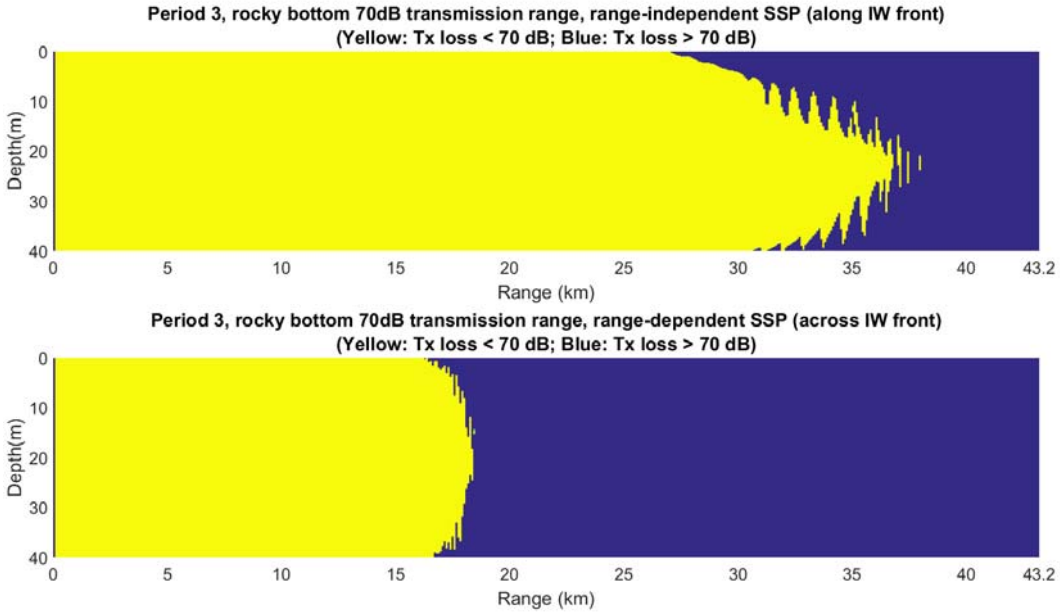

Figure 26b. Period 3—Sandy Bottom 70 dB Transmission Range for a Range-Independent SSP and a Range-Dependent SSP.

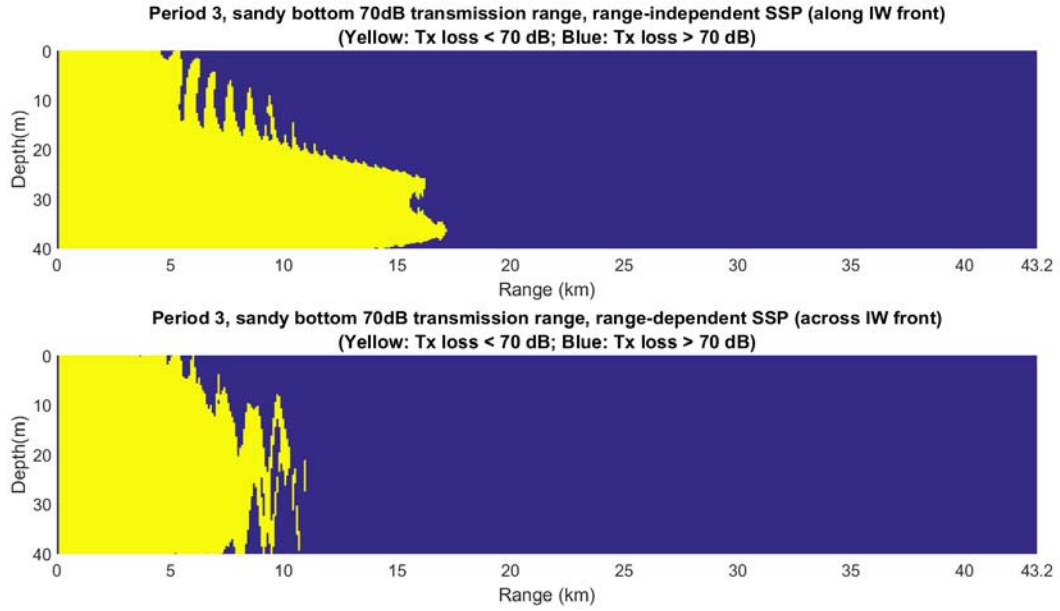

Figure 26c. Period 3—Muddy Bottom 70 dB Transmission Range for a Range-Independent SSP and a Range-Dependent SSP.

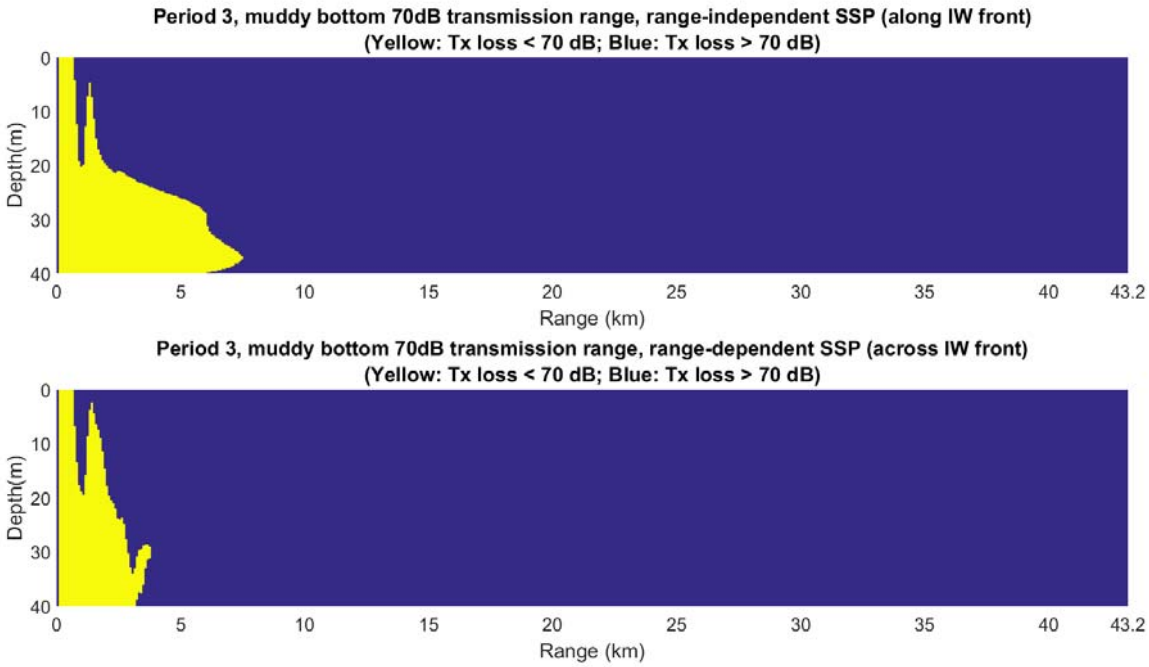

D. PERIOD 4: INTERNAL TIDES WITH LARGE TEMPERATURE DIFFERENCE, FEW SOLITONS

Period 4 (yeardays 200.6–202.9) was characterized by well-defined internal tides, with a relatively large temperature difference of 5.5°C (from 10.5 to 16°C) between the bottom and the surface of the water, and few solitons (fewer than 5 solitons a day, refer to Figure 8). The sound speed profile ranged from approximately 1492 m/s to 1508 m/s. For period 4a (yeardays 200.6–202.6), the sound source was placed at the center of a cold front of an internal tide (Figure 27), while period 4b (yeardays 200.9–202.9) had the sound source placed in the center of the warm front of the same internal tide (Figure 30). The objective was to determine if there are significant differences in sound attenuation when a sound source is in the different temperature fronts of an internal tide.

For period 4a, the transmission loss plots for the three types of seabed are shown in Figure 28. The 70 dB transmission range plots are shown in Figure 29. For a rocky bottom, the 70 dB transmission range was reduced from 39.2 km for along internal wave front propagation to 18.3 km for across internal wave front propagation. For a sandy

bottom, the range was reduced from 19.5 km to 6.7 km. For a muddy bottom, the range was reduced from 4.3 km to 2.0 km.

For period 4b, the transmission loss plots for the three types of seabed are shown in Figure 31. The 70 dB transmission range plots are shown in Figure 32. For a rocky bottom, the 70 dB transmission range was reduced from 37.8 km for along internal wave front propagation to 19.2 km for across internal wave front propagation. For a sandy bottom, the range was reduced from 10.0 km to 5.8 km. For a muddy bottom, the range remains the same at 2.0 km.

It can be observed that for a sandy and a muddy seabed, having a sound source in the cold or warm front of an internal tide results in a large variability in along internal wave front sound propagation ranges. For a sandy bottom, the along cold front 70 dB transmission range was 19.5 km, while the along warm front 70 dB transmission range was 10.0 km. For a muddy bottom, the along cold front 70 dB transmission range was 4.3 km, while the along warm front 70 dB transmission range was 2.0 km.

Figure 27. Period 4a—Range-Independent SSP (top), Range-Dependent SSP (bottom) 0 km at Yearday 200.6 (Cold Front of IW).

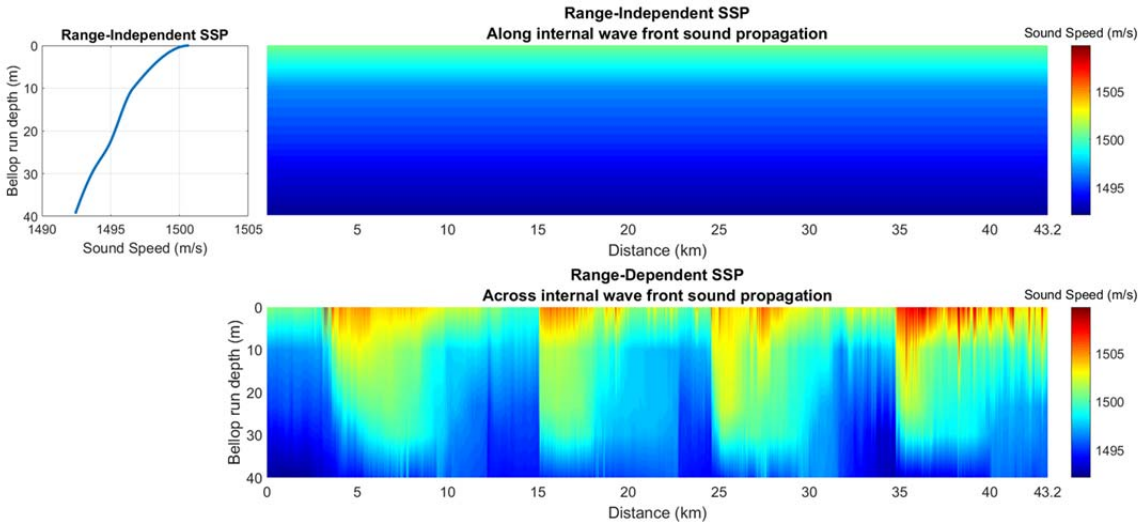

Figure 28. Period 4a—Transmission Loss for a Rocky, Sandy, and Muddy Seabed. (Figures 28a–c).

Figure 28a. Period 4a—Rocky Bottom Transmission Loss through Range-Independent SSP and Range-Dependent SSP.

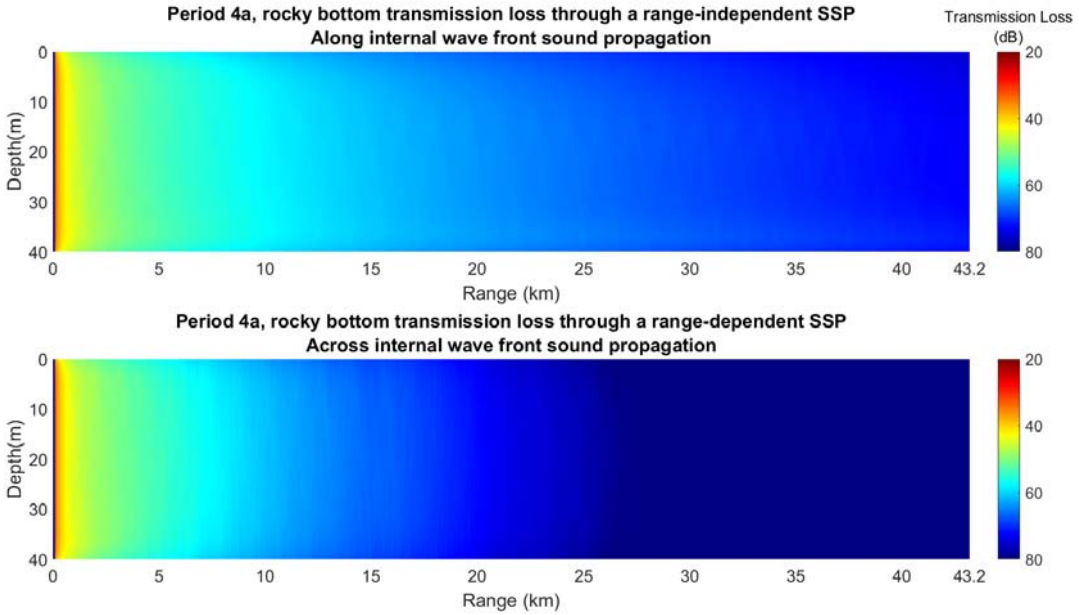

Figure 28b. Period 4a—Sandy Bottom Transmission Loss through Range-Independent SSP and Range-Dependent SSP.

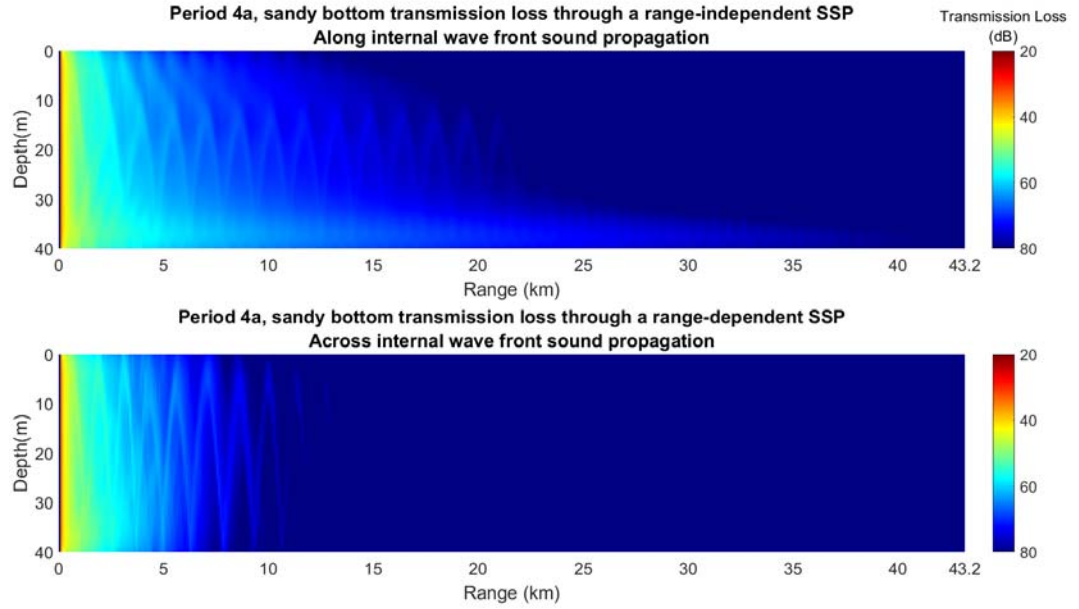

Figure 28c. Period 4a—Muddy Bottom Transmission Loss through Range-Independent SSP and Range-Dependent SSP.

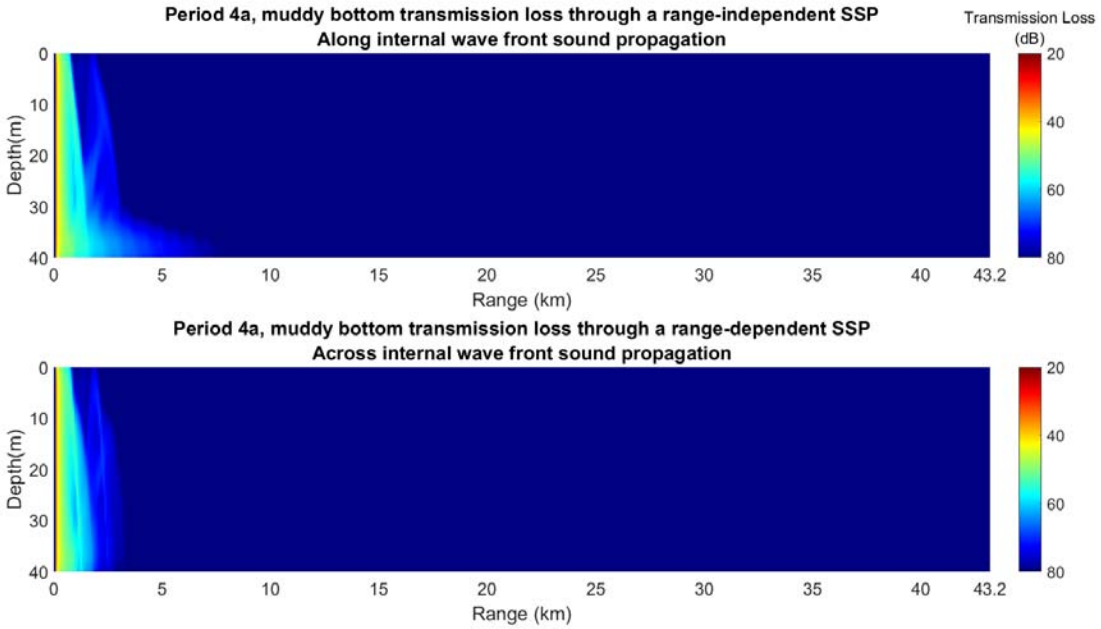

Figure 29. Period 4a—70 dB Transmission Loss Range for a Rocky, Sandy, and Muddy Seabed. (Figures 29a–c).

Figure 29a. Period 4a—Rocky Bottom 70 dB Transmission Range for a Range-Independent SSP and a Range-Dependent SSP.

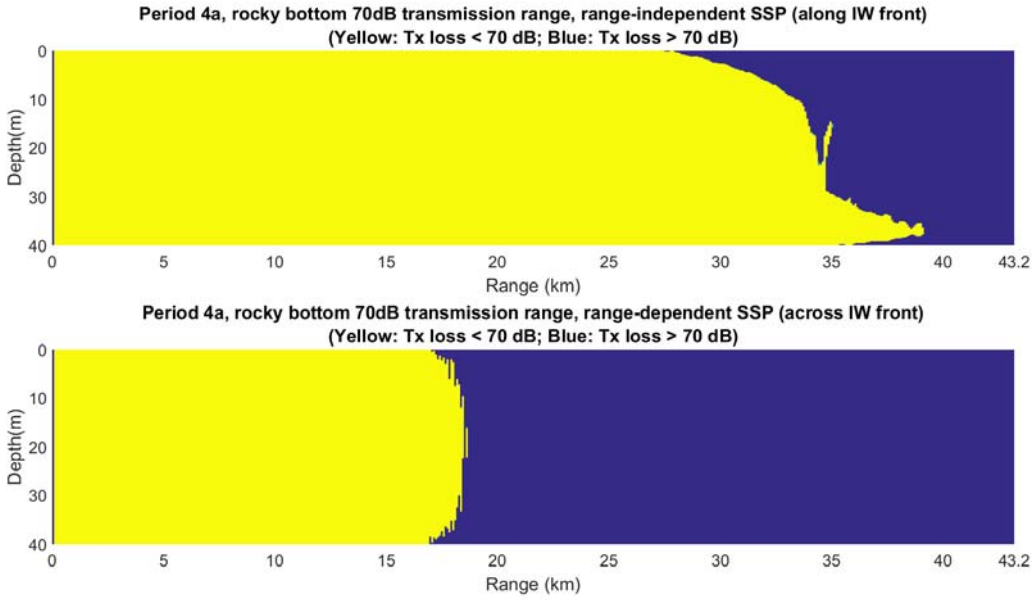

Figure 29b. Period 4a—Sandy Bottom 70 dB Transmission Range for a Range-Independent SSP and a Range-Dependent SSP.

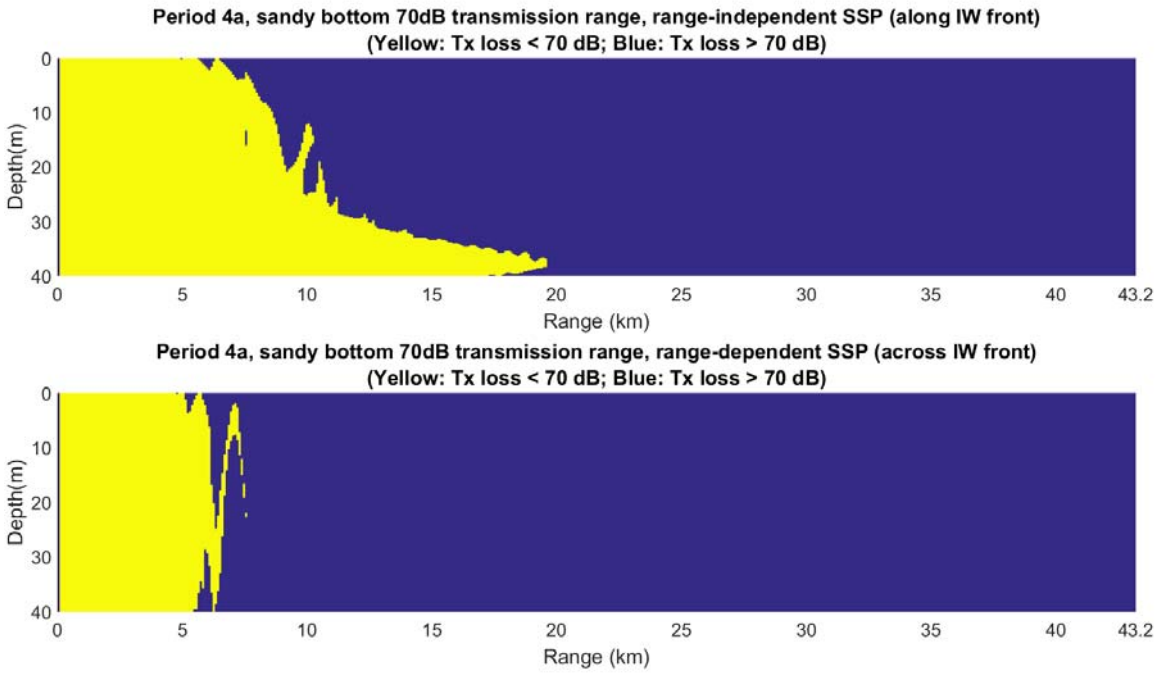

Figure 29c. Period 4a—Muddy Bottom 70 dB Transmission Range for a Range-Independent SSP and a Range-Dependent SSP.

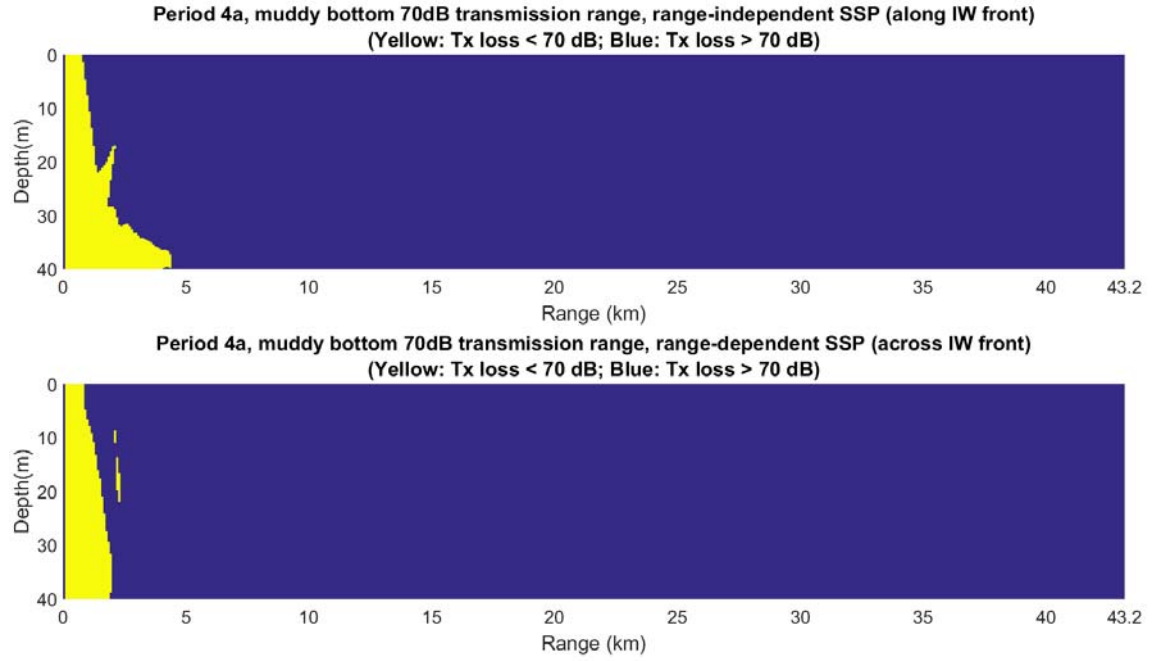

Figure 30. Period 4b—Range-Independent SSP (top), Range-Dependent SSP (bottom) 0 km at Yearday 200.9 (Warm Front of IW).

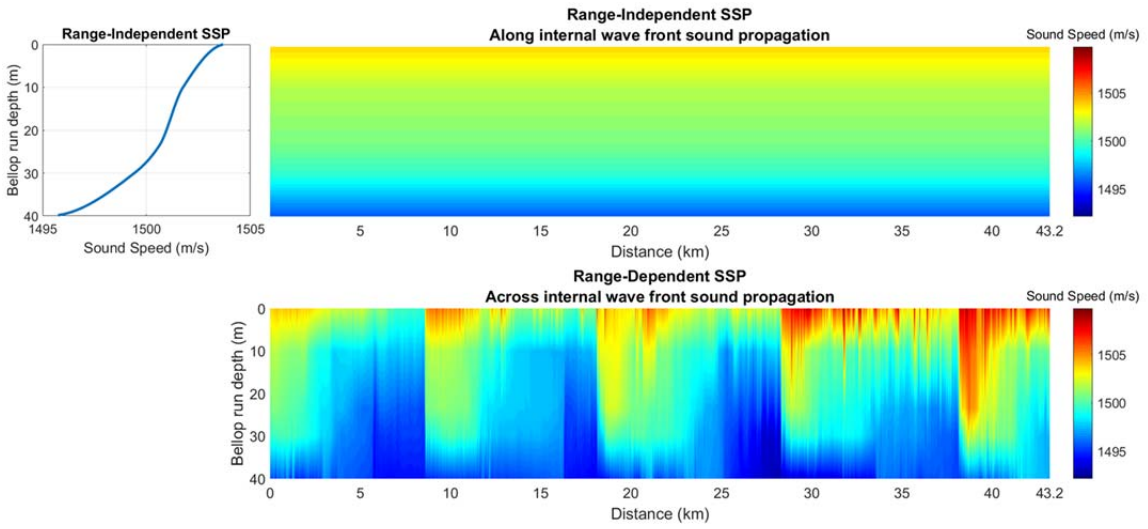

Figure 31. Period 4b—Transmission Loss for a Rocky, Sandy, and Muddy Seabed. (Figures 31a–c).

Figure 31a. Period 4b—Rocky Bottom Transmission Loss through Range-Independent SSP and Range-Dependent SSP.

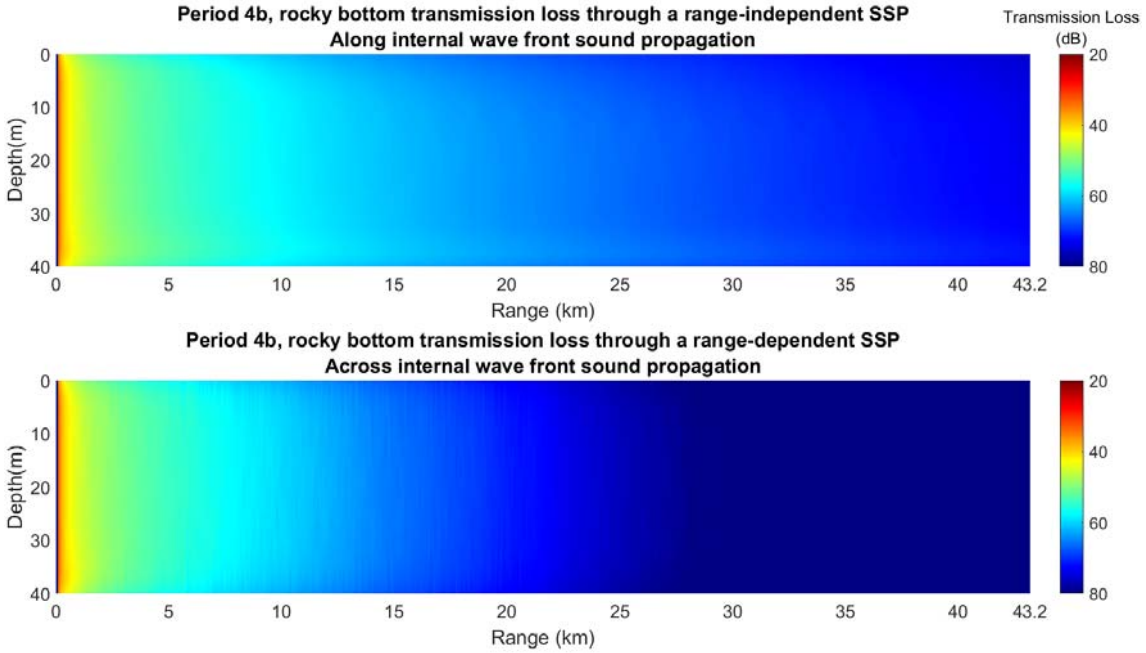

Figure 31b. Period 4b—Sandy Bottom Transmission Loss through Range-Independent SSP and Range-Dependent SSP.

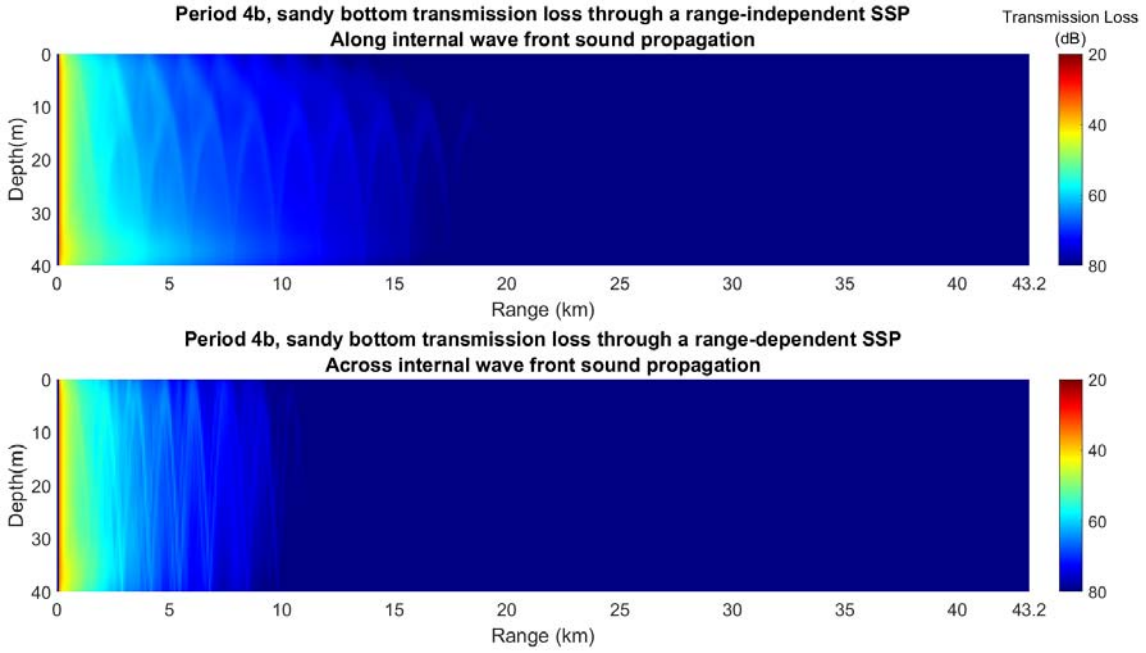

Figure 31c. Period 4b—Muddy Bottom Transmission Loss through Range-Independent SSP and Range-Dependent SSP.

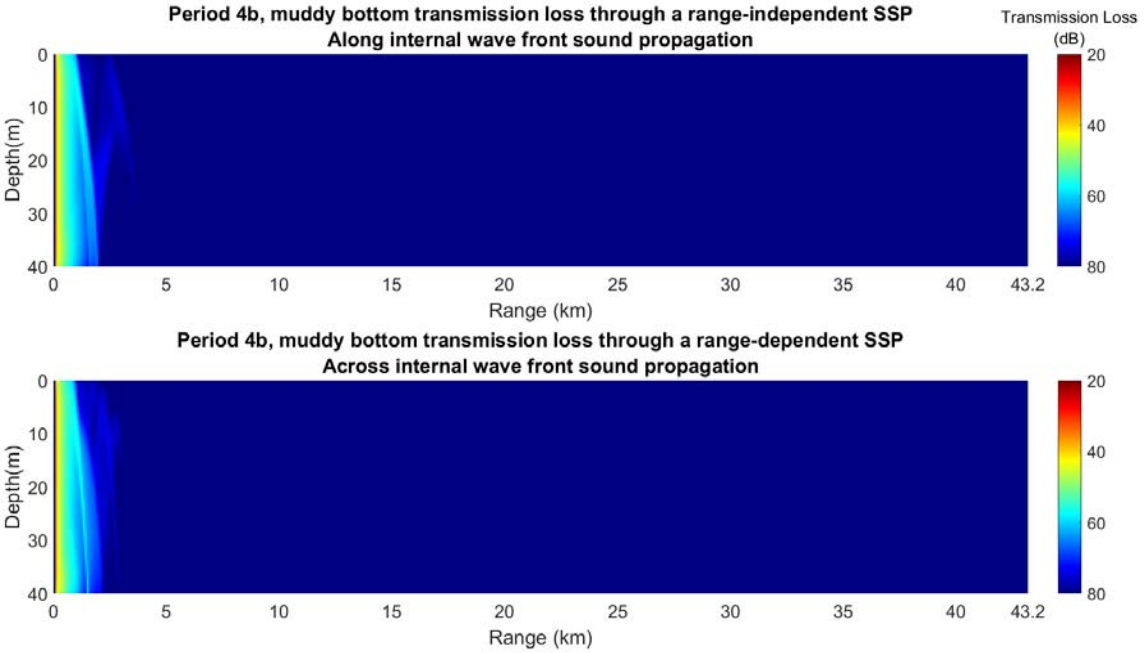

Figure 32. Period 4b—Transmission Loss Range for a Rocky, Sandy, and Muddy Seabed. (Figures 32a–c).

Figure 32a. Period 4b—Rocky Bottom 70 dB Transmission Range for a Range-Independent SSP and a Range-Dependent SSP.

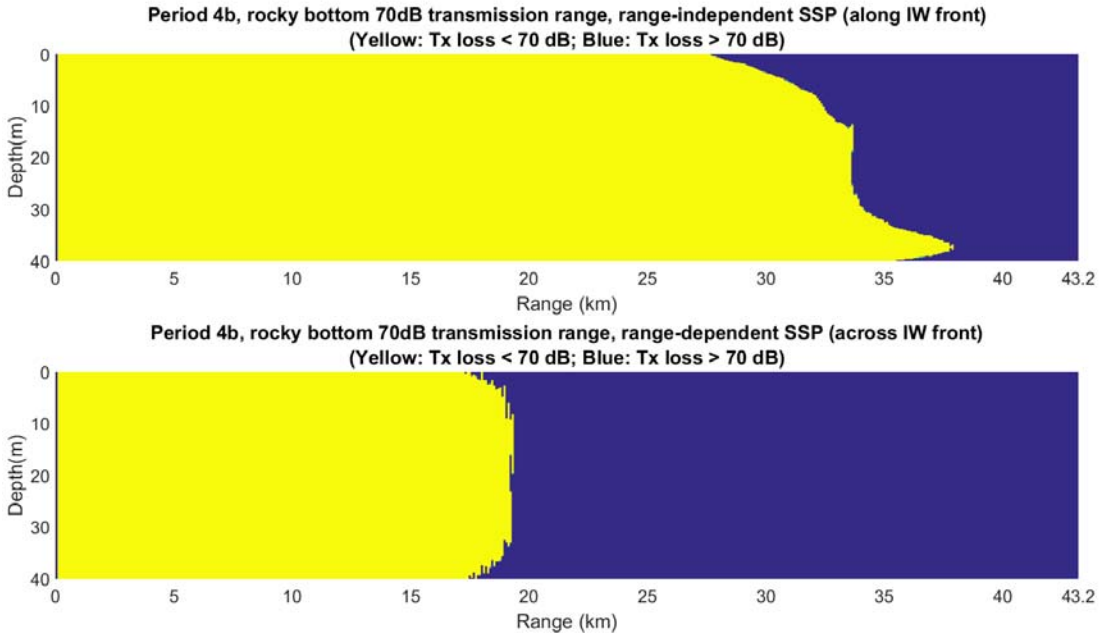

Figure 32b. Period 4b—Sandy Bottom 70 dB Transmission Range for a Range-Independent SSP and a Range-Dependent SSP.

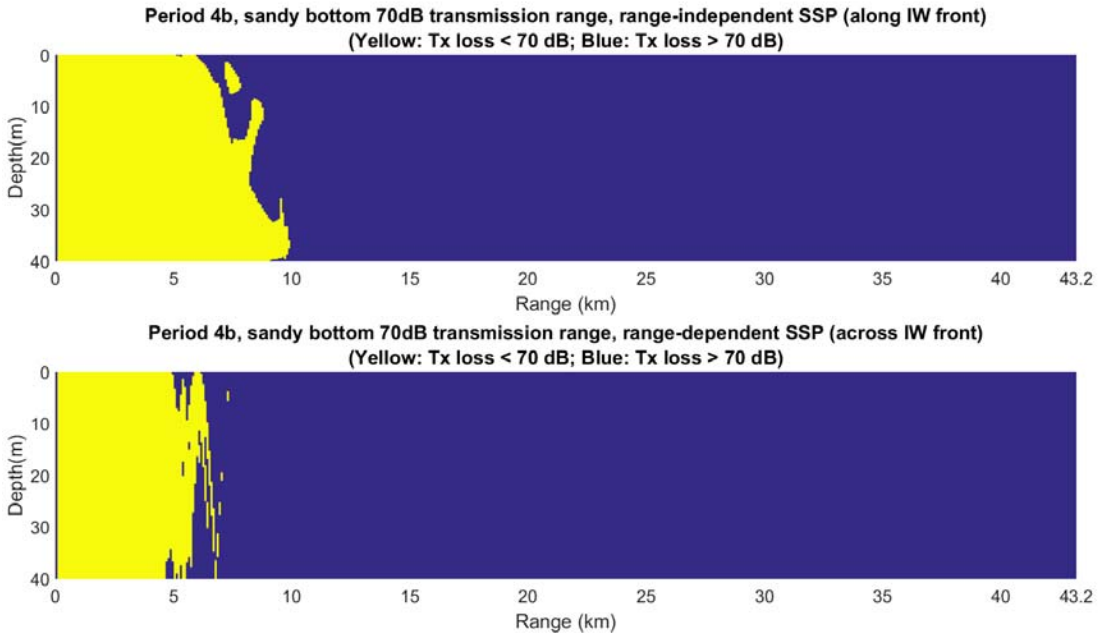

Figure 32c. Period 4b—Muddy Bottom 70 dB Transmission Range for a Range-Independent SSP and a Range-Dependent SSP.

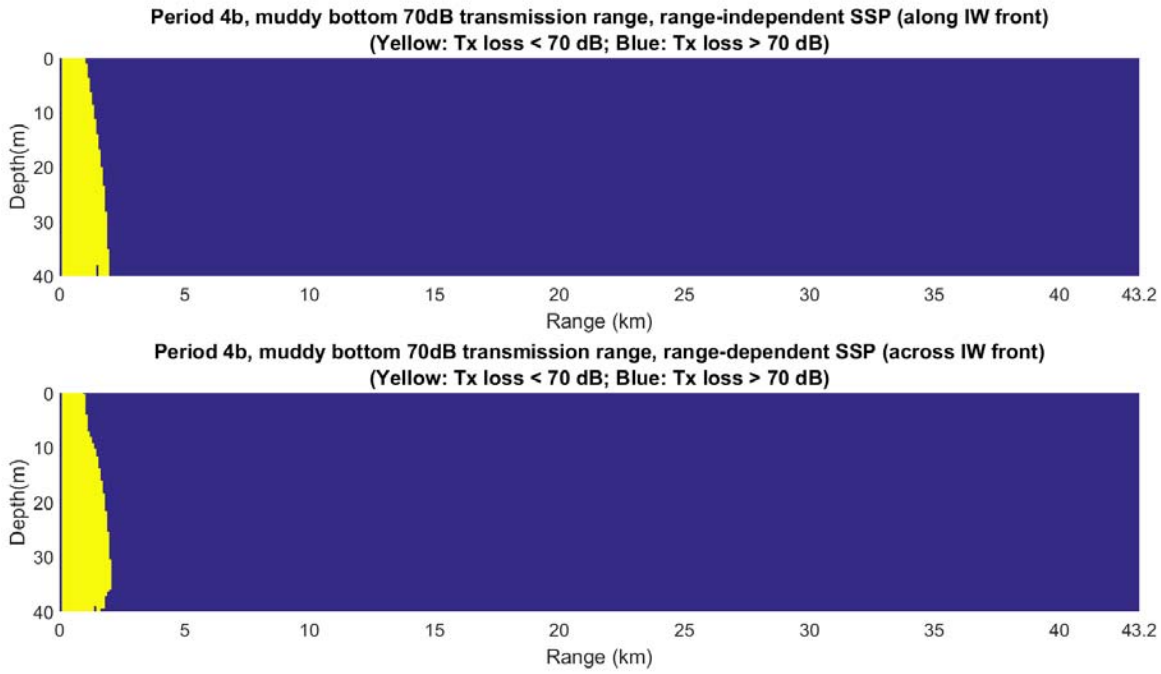

E. PERIOD 5: IN THE WARM AND COLD FRONT OF A STEEP TIDAL BORE

Period 5 was at approximately yearday 174.22, at the warm and cold interface of a steep-face tidal bore. Two simulation runs were conducted at data points that were 5 minutes or 75 m apart, with one data point at the warm front of the tidal bore and the other at the cold front of the tidal bore. The exact time of analysis and the 70 dB transmission range for a range-independent SSP and a range-dependent SSP are shown in Figure 33 and Figure 34, with Figure 31 starting in the warm front and Figure 32 starting in the cold front. A sandy bottom was used in the analysis.

While the range-dependent SSP (across internal wave fronts) did not show much change in the 70 dB transmission range between the two simulation time periods (8.3 km and 8.9 km), it was a different story for the range-independent SSP (along internal wave fronts). For the range-independent SSP the coming of the cold front of the internal tidal bore to displace the warmer waters resulted in the 70 dB transmission range increasing from 12.1 km to 32.1 km in just 5 minutes or just 75 m apart.

Figure 33. Period 5—Sandy Bottom 70 dB Transmission Range at the Warm Front of a Tidal Bore.

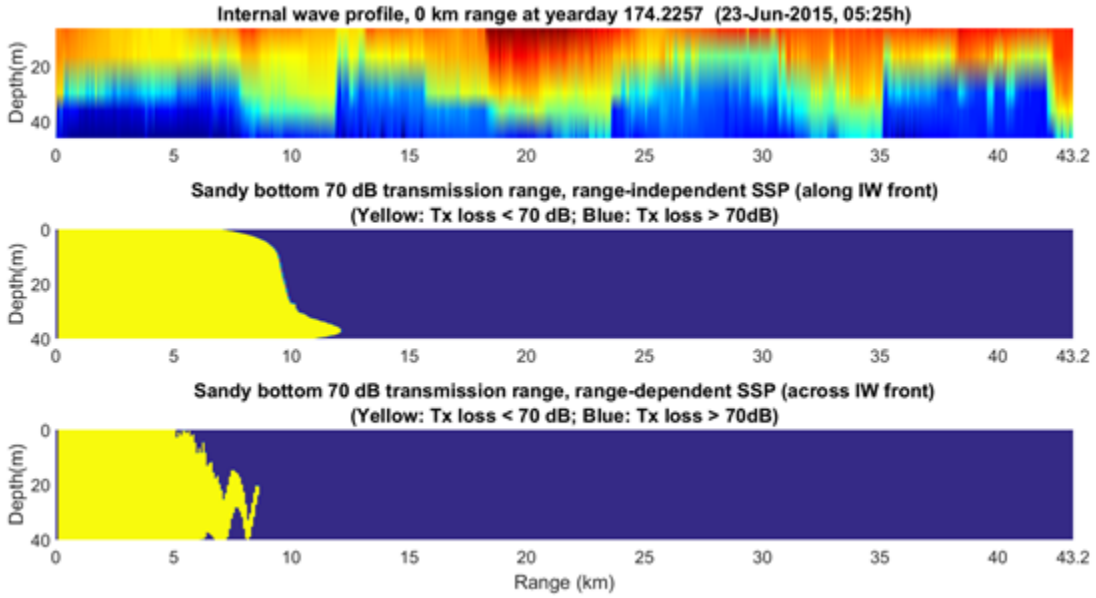

Figure 34. Period 5—Sandy Bottom 70 dB Transmission Range at the Cold Front of a Tidal Bore.

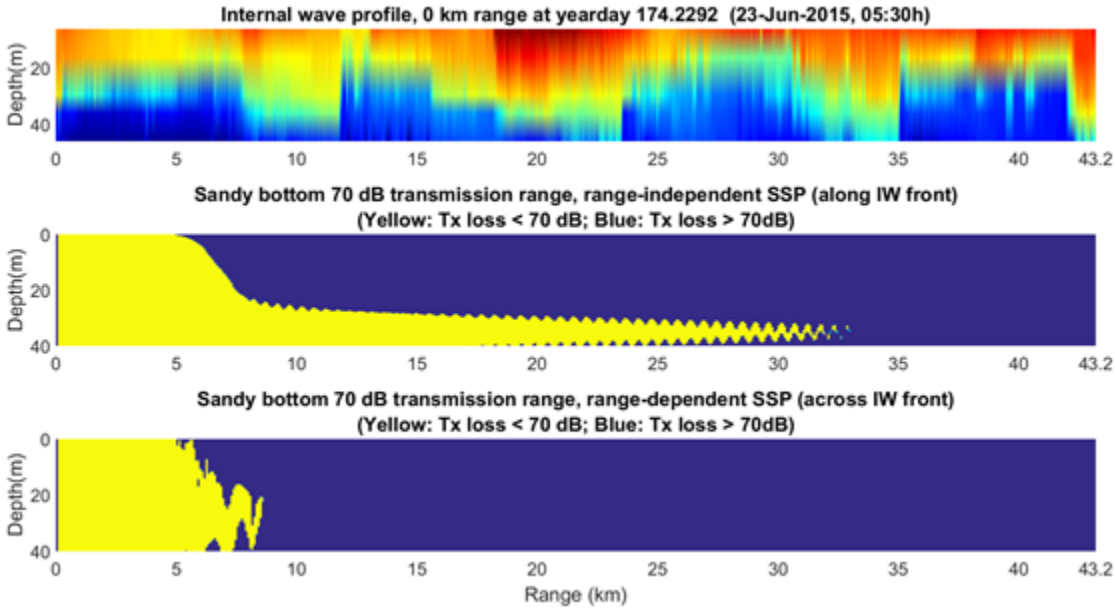

F. SUMMARY AND INTERPRETATION OF SIMULATION RESULTS

The results of the transmission loss runs are summarized in Table 4.

Table 4. Transmission Ranges for the Various Time Periods.

Period	Centered yearday	Internal tide	Solitons	70 dB transmission loss range
1	175–177	-Well-defined -Small temperature difference (2.5°C)	Few	Seabed: Rocky — Along IW: 40.0 km — Across IW: 21.5 km — % change: -46% Seabed: Sandy — Along IW: 27.3 km — Across IW: 6.2 km — % change: -77% Seabed: Muddy — Along IW: 26.5 km — Across IW: 2.5 km — % change: -91%
2	205–207	-Well-defined -Large temperature difference (7°C)	Many	Seabed: Rocky — Along IW: 37.5 km — Across IW: 18.3 km — % change: -51% Seabed: Sandy — Along IW: 12.2 km — Across IW: 6.5 km — % change: -47% Seabed: Muddy — Along IW: 1.8 km — Across IW: 2.5 km — % change: 39%
3	210–212	-Weak -Large temperature difference (6°C)	Many	Seabed: Rocky — Along IW: 36.8 km — Across IW: 18.5 km — % change: -50% Seabed: Sandy — Along IW: 17.2 km — Across IW: 9.5 km — % change: -45% Seabed: Muddy — Along IW: 7.5 km — Across IW: 3.7 km — % change: -51%
4a	200.6–202.6 Cold front of IW	-Well-defined -Fairly large temperature difference (5°C)	Few	Seabed: Rocky — Along IW: 39.2 km — Across IW: 18.3 km — % change: -53% Seabed: Sandy — Along IW: 19.5 km — Across IW: 6.7 km — % change: -66% Seabed: Muddy — Along IW: 4.3 km — Across IW: 2.0 km — % change: -53%
4b	200.9–202.9 Warm front of IW	Same as period 4b	Same as period 4b	Seabed: Rocky — Along IW: 37.8 km — Across IW: 19.2 km — % change: -49% Seabed: Sandy — Along IW: 10.0 km — Across IW: 5.8 km — % change: -42% Seabed: Muddy — Along IW: 2.0 km — Across IW: 2.0 km — % change: 0%
5	174.2–176.2 Edge of tidal bore	Same as period 1	Same as period 1	Seabed: Sandy (warm) — Along IW: 12.0 km — Across IW: 8.3 km — % change: -31% Seabed: Sandy (cold) — Along IW: 32.0 km — Across IW: 8.5 km — % change: -73%

Referring to Table 5, for a rocky bottom, sound traveling across internal wave fronts (range-dependent SSP) had its 70 dB transmission loss range reduced between 46% to 53%, when compared to sound traveling along the internal wave front (range-independent SSP).

The along internal wave 70 dB transmission ranges were from 36.8 km to 40.0 km across the various time periods, giving a variability of 3.2 km. The across internal wave 70 dB transmission ranges were from 18.3 km to 21.5 km across the various time periods, giving a variability of 3.2 km.

Table 5. 70 dB Transmission Ranges for a Rocky Bottom.

Period	Unique characteristics	Along IW	Across IW	% change
1	-Sound source in a well-defined bottom cold layer -Internal tides only	40.0 km	21.5 km	-46%
2	-Internal tides and solitons	37.5 km	18.3 km	-51%
3	-Solitons only	36.8 km	18.5 km	-50%
4a	-Sound source in the cold front of an internal tide	39.2 km	18.3 km	-53%
4b	-Sound source in the warm front of an internal tide	37.8 km	19.2 km	-49%
	Variability:	3.2 km	3.2 km	

Referring to Table 6, for a sandy bottom, sound traveling across internal wave fronts (range-dependent SSP) had its 70 dB transmission loss range reduced between 31% to 77%, when compared to sound traveling along the internal wave front (range-independent SSP).

The along wave front 70 dB transmission ranges were from 10.0 km to 32.0 km, giving a variability of 22 km, while the across wave front transmission ranges were from 5.8 km to 9.5 km, giving a variability of 3.7 km. It can be observed that a sound source placed in the cold front of an internal wave supported an extended transmission range as compared to a sound source placed in the warm front of an internal wave, and this resulted in a large variability in the along internal wave front 70 dB transmission range

Table 6. 70 dB Transmission Ranges for a Sandy Bottom.

Period	Unique characteristics	Along IW	Across IW	% change
1	-Sound source in a well-defined bottom cold layer -Internal tides only	27.3 km	6.2 km	-77%
2	-Internal tides and solitons	12.2 km	6.5 km	-47%
3	-Solitons only	17.2 km	9.5 km	-45%
4a	-Sound source in the cold front of an internal tide	19.5 km	6.7 km	-66%
4b	-Sound source in the warm front of an internal tide	10.0 km	5.8 km	-42%
5a	-Sound source in the warm front of a tidal bore	12.1 km	8.3 km	-31%
5b	-Sound source in the cold front of a tidal bore	32.0 km	8.5 km	-73%
	Variability:	22.0 km	3.7 km	

Referring to Table 7, for a muddy bottom, the along internal wave front 70 dB transmission ranges were from 2.0 km to 26.5 km (24.5 km variability), while the across wave front transmission ranges were from 2.0 km to 3.7 km (1.7 km variability). The only instance where the muddy seabed could support a longer range 70 dB transmission range was in period 1, which had a thin well-defined cold bottom layer. If this period was removed from the analysis, the muddy bottom along wave front 70 dB transmission ranges would be from 2.0 km to 7.5 km (5.5 km variability).

As for percentage change in the 70 dB transmission range for the across internal wave fronts (range-dependent SSP) sound propagation as compared to the along internal wave fronts (range-independent SSP), a range gain of 39% (from 1.8 km to 2.5 km) was observed in period 2. This range gain only occurred when the along wave front sound propagation ranges were short (at approximately 2 km). The range gain could occur as when the grazing sound wave angle increases from beyond the Brewster angle, where all sound energy is absorbed by the muddy seabed, there will be some energy that will be reflected back into the water. All the other cases had range reduction from 0–91%.

Table 7. 70 dB Transmission Ranges for a Muddy Bottom.

Period	Unique characteristics	Along IW	Across IW	% change
1	-Sound source in a well-defined thin bottom cold layer -Internal tides only	26.5 km	2.5 km	-91%
2	-Internal tides and solitons	1.8 km	2.5 km	39%
3	-Solitons only	7.5 km	3.7 km	-51%
4a	-Sound source in the cold front of an internal tide	4.3 km	2.0 km	-53%
4b	-Sound source in the warm front of an internal tide	2.0 km	2.0 km	0%
	Variability:	24.5 km (5.5 km if period 1 is excluded)	1.7 km	

THIS PAGE INTENTIONALLY LEFT BLANK

VIII. HOW INTERNAL WAVES AFFECT SOUND TRAVEL PATHS

Observing that simulation runs that factored in the effects of internal waves generally resulted in greater transmission loss compared to simulation runs that do not account for the effects of internal waves, it would be logical to conclude that internal waves cause the sound waves to refract downward more. This leads them to strike the seabed at a larger grazing angle, resulting in fewer "rays" experiencing total internal reflection; for "rays" beyond the critical angle, it pushes them into a steeper grazing angle with a resulting smaller reflection coefficient.

To verify this hypothesis, a ray trace was done for period 4a, at a launch angle of 1° below the horizontal plane, as shown in Figure 35. The top ray trace was without the effects of internal waves, and the ray in the positive ranges (0 to 20 km) had 15 bottom bounces in the positive ranges before it exited the plot. For the lower ray trace plot, which accounted for internal waves, the ray in the positive ranges had 17 bottom bounces before it exited the plot, which is two more bottom interactions than the ray trace without internal waves. Comparing the internal wave ray trace plot with the SSP plot (Figure 35, bottom), it can be seen that when the sound wave passes through the warm front of an internal wave, at the 5–10 km region, with an associated larger temperature difference, sound waves get "depressed" more and strike the seabed at a faster rate than when passing through a colder mass of water. This would cause more transmission loss if the grazing angle is greater than the critical angle for which total internal reflection can occur for a rocky and sandy bottom.

As for the ray in the negative ranges of the plot (0 to -20 km), the top ray trace had 15 bounces, while the bottom ray trace had 14 bottom bounces, which was one fewer bottom bounces. Internal waves still caused more losses in this scenario as the ray trace without internal waves had the ray refracted downward at a constant depth of 20 m, while for the ray trace with internal waves, the ray got refracted downward mostly at shallower depths of less than 20 m. This means that the ray that experiences internal waves would have had a greater grazing angle when striking the bottom, which translates to more

losses overall, even when it had one fewer bottom interactions compared to the ray trace without the effects of internal waves.

Figure 35. Ray Trace without Internal Waves (top), Ray Trace with Internal Waves (middle), and Temperature Profile (bottom).

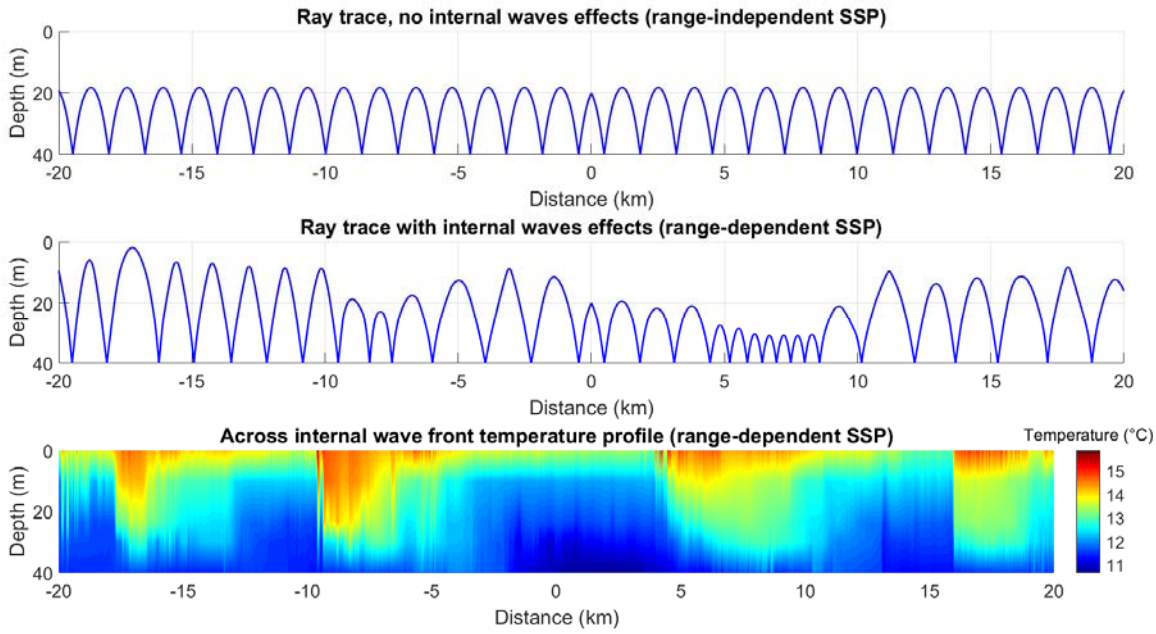

In conclusion, ray tracing of sound waves confirmed the hypothesis that internal waves cause sound waves to refract downward more, causing more bottom interactions over the same distance or increasing the angle of grazing when striking the seabed. The net effect was more losses over the same distance as compared to a model without internal waves. This would explain why simulations that accounted for the effects of internal waves via range-dependent SSPs resulted in higher transmission loss as compared to simulations that did not account for the effects of internal waves.

IX. CONCLUSION

The simulation of the effects of internal waves on sound propagation, based on real world internal wave data, showed that internal waves introduced great variability in sound propagation ranges in the shallow waters of the continental shelves, as the internal waves modulate the SSP in time scales as short as a few minutes.

Assuming internal waves in the experiment area, which are propagating in the west-east direction, have plane wave structures, sound waves propagating in a northerly/southerly direction will then run along or in parallel to the wave fronts of these internal waves (see Figure 36). In this scenario, the location of the sound source with respect to the warm or cold front of an internal wave front has a great effect on the sound transmission range, with a cold front allowing a farther transmission range compared to a warm front. In one of the simulation runs where the warm and cold front interface of an internal wave was in the form of a steep tidal bore, a transmission range of 32.0 km was reached in the cold front of the bore, but dropped to 12.0 km in the warm front of the bore, which was in a data point just 5 minutes or 75 m apart.

Figure 36. Along Wave Front Variability in Sound Transmission Range Due to the Warm and Cold Fronts of Internal Waves.

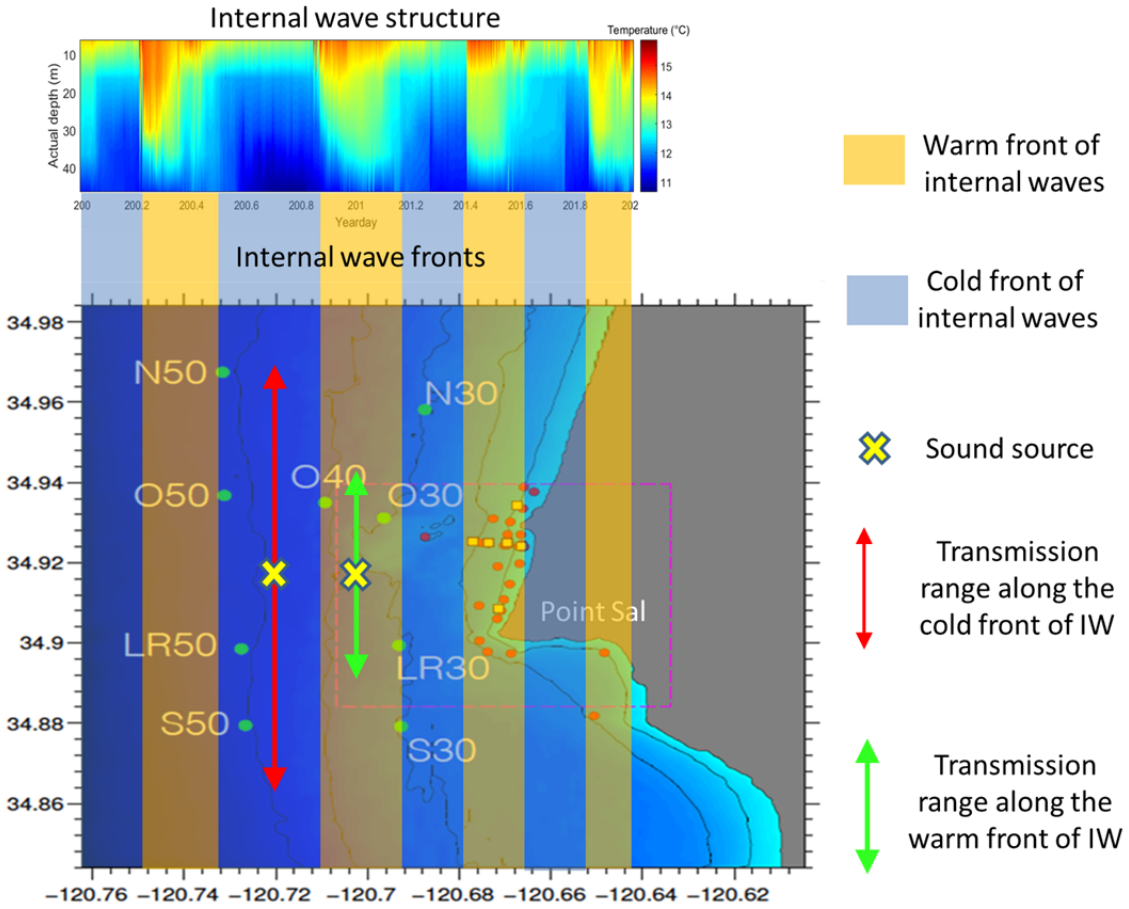

Sound waves propagating along the warm front of an internal wave have greater attenuation compared to sound waves propagating along the cold front of an internal wave.

For sound waves propagating in an easterly/westerly direction, they will cut across the wave fronts of internal waves, resulting in them having shorter transmission ranges as compared to sound waves of the same power level propagating in the northerly/southerly direction (i.e., in parallel to the wave fronts of the internal waves). This scenario is illustrated in Figure 37. In simulation runs conducted using a sandy seabed, this resulted in a 31–77% reduction in transmission ranges (from 10.0–32.0 km to 5.8–9.5 km) when compared to sound waves that travel along the internal wave fronts.

Figure 37. Across Wave Front Sound Transmission Range Reduction Effects of Internal Wave.

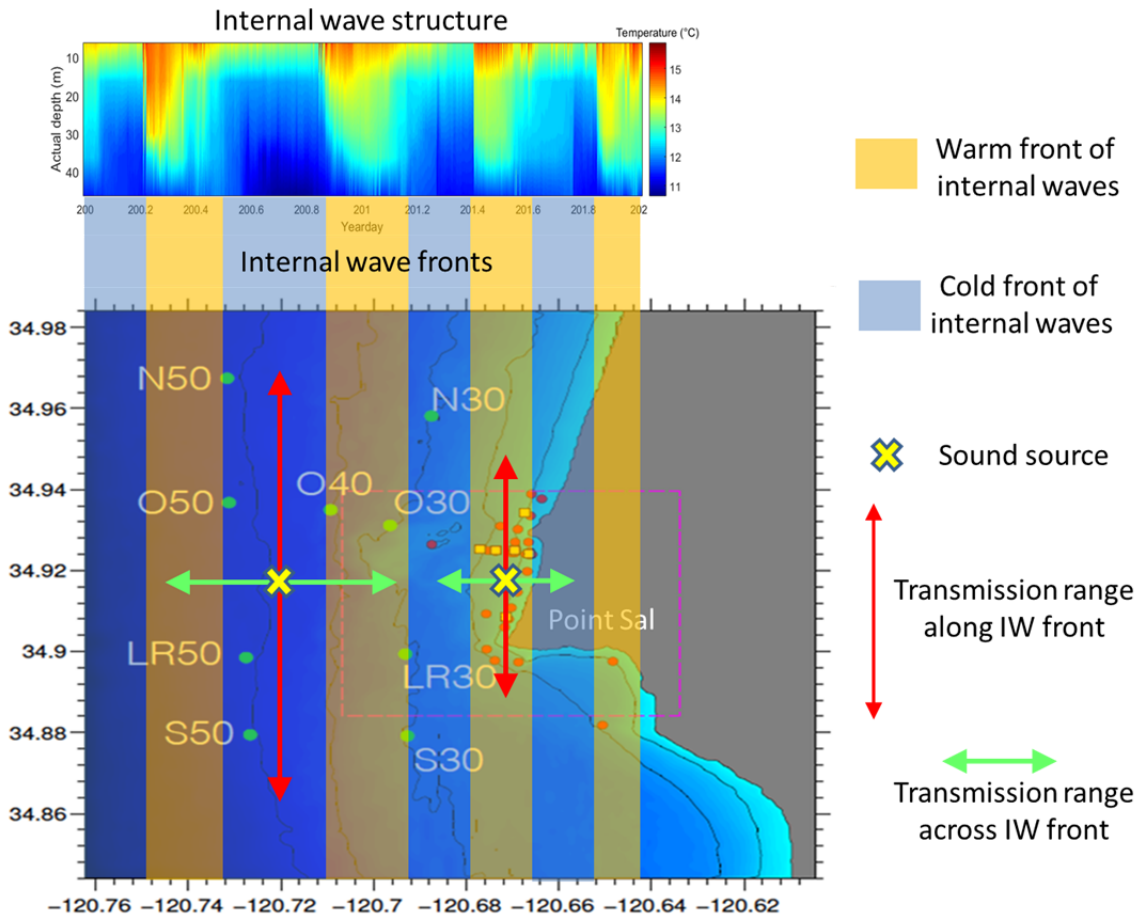

Sound waves have greater attenuation when propagating across internal wave fronts when compared to propagating along internal wave fronts.

In conclusion, for sound propagation along internal wave fronts, internal waves cause great variability in propagation ranges, with cold fronts allowing farther propagation range than warm fronts. As for sound propagation across internal wave fronts, internal waves cause them to have a shorter propagation range compared to the sound waves of the same power level that are traveling along an internal wave front.

Hence, the current practice of dropping an XBT or CDT into one spot to get the SSP for that location, and using that one SSP for "range of the day" estimation of acoustical systems performance, with the underlying assumption that the SSP does not

change with location, range, or time may not be the best approach in the shallow waters of the continental shelves.

Going forward, in scenarios where an accurate estimation of acoustical system range performance is important for "mission success," such as in the search for and location of an aircraft "black box" that is suspected to be on the seabed, the effects of internal waves on the "black box" underwater sound beacon transmission range would have to be accounted for in the modeling and simulation runs during "mission planning," to ensure there are no inadvertent gaps in the search operation.

This study conducted analyses of the effects of internal waves on sound propagation using the assumption that internal wave fronts take on the structure of plane waves. While this allowed a baseline generic assessment of the effects of internal waves on sound propagation, internal waves in the shallow waters of the continental shelves have been observed to have more complex structures that are closely tied to an area's bathymetry (Jackson 2004). Hence, to accurately account for the effects of internal waves on sound propagation ranges, further data measurements are required at the locations where underwater acoustical operations have to be carried out.

LIST OF REFERENCES

Apel, J., M. Badiey, C. S. Chiu, S. Finnette, R. Headrick, J. Kemp, J. Lynch, A. Newhall, M. Orr, B. Pasewark, D. Teilbuerger, A. Turgut, K. von der Heydt, and S. Wolf, 1997: An overview of the 1995 SWARM shallow water internal wave acoustic scattering experiment. IEEE 1. *Oceanic Eng.*, **22**, 465–500.

Apel, J., L. A. Ostrovsky, Y. A. Stepanyants, and J. F. Lynch, 2007: Internal solitons in the ocean and their effect on underwater sound. *J. Acoust. Soc. Am.*, **121**, 695–722.

Colosi, J. A., J. MacMahan, and T. Freismuth, 2016: An overview of the 2015 Point Sal Inner Shelf Experiment (PSIEX): In-situ observations of temperature and current fields. PowerPoint slides. Department of Oceanography, Naval Postgraduate School.

Colosi, J. A., 2015: *Sound Propagation through the Stochastic Ocean*. Cambridge University Press, 424 pp.

Etter, P. C., 2013: *Underwater Acoustic Modeling and Simulation* (4th edition). Taylor & Francis, 554 pp.

Gerkema, T., and J. T. F. Zimmerman, 2008: An introduction to internal waves. Lecture Notes, R. Neth. Inst. for Sea Res., Den Burg, 207 pp.

Jackson, C. R., 2004: *An Atlas of Internal Solitary-like Waves and Their Properties* (2nd edition). Global Ocean Associates, 560 pp.

Jensen, F. B., W. A. Kuperman, M. B. Porter, and H. Schmidt, 1997: *Computational Ocean Acoustics*. American Inst. of Physics, 595 pp.

Kapolka, D., 2015: PH3401—Introduction to the sonar equations. PowerPoint lecture notes. Department of Physics, Naval Postgraduate School.

Mackenzie, K. V, 1981: Nine-term equation for sound speed in the oceans. *J. Acoust. Soc. Am.*, **70**, 807.

Marwoto, B., 2015: Horizontal anisotropy and seasonal variation of acoustic fluctuations observed during the 2010–2011 Philippine Sea experiment. M.S. thesis, Department of Oceanography, Naval Postgraduate School, 47 pp.

Porter, M. B., 2011: The BELLHOP manual and user's guide preliminary draft. Heat, Light, and Sound Research, Inc. [Available online at http://oalib.hlsresearch.com/Rays/.]

Porter, M. B., and H. P. Bucker, 1987: Gaussian beam tracing for computing ocean acoustic fields. *J. Acoust. Soc. Am.*, **82**, 4, 1349–1359.

Robert, J. W., and J. T. William, 1983: Estimation of Brunt-Väisälä Frequency from temperature profiles. *J. Phys. Oceanogr.*, **13**, 2236–2240.

Rodríguez, O. C., 2008: General description of the BELLHOP ray tracing program. University of Algarve. [Available online at http://oalib.hlsresearch.com/Rays/.]

Thorp, W. H., 1967: Analytic description of the low-frequency attenuation coefficient. *J. Acoust. Soc. Amer.*, **88**, 335–349.

Urick, R. J., 1983: *Principles of Underwater Sound* (3rd edition). Peninsula Publishing, 423 pp.

Wenz, G. M., 1962: Acoustic ambient noise in the ocean: Spectra and sources. *J. Acoust. Soc. Am.*, **34**, 12, 1936–1956.

Zhou, J. X., X. Z. Zhang, and P. H. Rogers, 1991: Resonant interaction of sound wave with internal solitons in the coastal zone. *J. Acoust. Soc. Am.*, **90**, 4, 2042–2054.

INITIAL DISTRIBUTION LIST

1. Defense Technical Information Center
   Ft. Belvoir, Virginia

2. Dudley Knox Library
   Naval Postgraduate School
   Monterey, California